frontiers | Frontiers in Earth Science

TYPE Original Research
PUBLISHED 13 December 2022
DOI 10.3389/feart.2022.1031239

OPEN ACCESS

EDITED BY
Ren-Xu Chen,
University of Science and Technology of China, China

REVIEWED BY
Theo Ntaflos,
University of Vienna, Austria
Davide Lenaz,
University of Trieste, Italy

*CORRESPONDENCE
Harilaos Tsikos,
htsikos@upatras.gr

SPECIALTY SECTION
This article was submitted to Petrology, a section of the journal Frontiers in Earth Science

RECEIVED 29 August 2022
ACCEPTED 28 November 2022
PUBLISHED 13 December 2022

CITATION
Sideridis A, Tsikouras B, Tsitsanis P, Koutsovitis P, Zaccarini F, Hauzenberger C, Tsikos H and Hatzipanagiotou K (2022), Post-magmatic processes recorded in bimodal chromitites of the East Chalkidiki meta-ultramafic bodies, Gomati and Nea Roda, Northern Greece.
Front. Earth Sci. 10:1031239.
doi: 10.3389/feart.2022.1031239

Post-magmatic processes recorded in bimodal chromitites of the East Chalkidiki meta-ultramafic bodies, Gomati and Nea Roda, Northern Greece

Alkiviadis Sideridis[1], Basilios Tsikouras[2], Pavlos Tsitsanis[3], Petros Koutsovitis[1], Federica Zaccarini[2], Christoph Hauzenberger[4], Harilaos Tsikos[1]* and Konstantin Hatzipanagiotou[1]

[1]Section of Earth Materials, Department of Geology, University of Patras, Patras, Greece, [2]Faculty of Science, Geosciences Programme, Universiti Brunei Darussalam, Bandar Seri Begawan, Brunei Darussalam, [3]Independent Researcher, Makedonias, Nea Moudania, Greece, [4]NAWI Graz Geocenter, University of Graz, Universitätsplatz, Graz, Austria

The meta-ultramafic bodies of Gomati and Nea Roda are situated in the Serbomacedonian Massif. They demonstrate bimodal character in terms of chromitite chemistry with both Cr- and Al-rich chromitites outcropping in proximity, with no obvious tectonic structure intercepting those two varieties. Based on the trace element abundances in spinel grains, metamorphosis reached amphibolite facies, forming porous spinel. Chromitite-hosted chlorite and garnet chemistry correlates with greenschist facies temperatures and formation of zoned spinel grains. Despite the metamorphic overprint, some of the primary features of the chromitites have been preserved. The PGE contents demonstrate an increase in Pd/Ir ratios in some chromitites pointing to fractionation, whereas low ratios of mostly Cr-rich chromitites point to partial melting being the main mechanism that controls PGE mineralization. The normalized trace element patterns of spinel-group minerals revealed that Al-rich chromitites were generated in spreading settings in a back-arc and the Cr-rich counterparts in SSZ environment. The parental melts of Al-rich and Cr-rich chromitites demonstrate MORB and boninitic affinities, respectively. The meta-ultramafic protoliths were modified within a subduction zone, with significant input of a sedimentary source, as confirmed by the chemistry of serpentinite, diopside and Sb-mineralization. These results suggest common geotectonic processes within the Rhodope and the Serbomacedonian massif, that have affected the ultramafic bodies and chromitite occurrences.

KEYWORDS

podiform chromitite, platinum-group minerals, platinum-group elements, subduction zone, Serbomacedonian massif, metamorphosis, meta-ophiolites, bimodal chromitites

1 Introduction

The ultramafic bodies of Gomati and Nea Roda of the Therma-Volvi-Gomati complex (TVG), situated in eastern Chalkidiki, Greece, are enigmatic components of the Serbomacedonian Massif (SMM), which is regarded as a metamorphic crustal segment of the internal Hellenides. Early research regarded the metabasic-metaultrabasic TVG (Therma, Volvi and Gomati occurrences) complex as a result of an *in-situ* Jurassic-Cretaceous related rifting (Dixon and Dimitriadis, 1984), formed in supra-subduction zone (SSZ) settings (Tsikouras and Hatzipanagiotou, 1998). However, recently Bonev et al. (2018) recognized limited SSZ components and confirmed a Triassic rift origin for the TVG complex. The same authors add the neighboring Nea Roda ultramafic body in the same complex and highlight their role as ocean-continent transition zone (OCT), against their previous view on the TVG complex as proto-ophiolites (Bonev and Dilek, 2010a). Both Gomati and Nea Roda ultramafic bodies contain podiform chromitite occurrences. The Gomati complex was considered hosting Al-rich chromitite, whereas the Nea Roda one hosts Cr-rich chromitite (Michailidis and Soldatos, 1995; Economou-Eliopoulos, 1996). These outcrops have experienced metamorphism at upper greenschist-lower amphibolite and greenschist facies, respectively (Christodoulou and Hirst, 1985; Michailidis and Soldatos, 1995).

The formation of podiform chromitites and their compositional traits are linked to SSZ (Cr-rich chromitite) or mid-ocean ridge (MOR) (Al-rich chromitite) (Dick and Bullen, 1984; Kamenetsky et al., 2001; Arai et al., 2006). In these settings, crystallization of mafic magmas or melt-rock interaction will lead to the formation of podiform chromitites within the mantle portion of ophiolitic sequences (Zhou et al., 1994; Xiong et al., 2017). With respect to their geochemical features, the parental melts of Cr-rich and Al-rich chromitites have boninitic and tholeiitic affinities, respectively (Maurel and Maurel, 1982; Uysal et al., 2009). Occasionally, both types can coexist within the same complex or in close proximity, which is a rather common phenomenon in the Tethyan ophiolites (Xiong et al., 2017, 2018).

The most common magmatic silicates hosted within podiform chromitites are olivine and pyroxene accompanied by less abundant amphibole and phlogopite (Melcher et al., 1997; Uysal et al., 2009). Podiform chromitites may contain a suite of accessory magmatic phases, such as Ni-Fe-Cu sulfides and platinum group minerals (PGM), making them a potential tool to unraveling the processes that lead to their formation at high temperatures (Melcher et al., 1997; Uysal et al., 2009). However, ophiolites in many cases are subjected to low-T alteration and metasomatic processes or high grade metamorphism, which may affect the chromitite bodies, causing mineralogical changes (Zaccarini et al., 2005; González-Jiménez et al., 2015; Xiong et al., 2021). Primary silicates will transform into serpentine, talc, chlorite and to a lesser extent into secondary Cr-bearing garnet (Tsoupas and Economou-Eliopoulos, 2008; Kapsiotis et al., 2017; Farré-de-Pablo et al., 2021). Although spinel and PGM are usually less susceptible to hydrothermal and metamorphic overprints (Sideridis et al., 2022), they may produce unique textures and change their primary compositional and mineralogical assemblages (Zaccarini et al., 2005; Kapsiotis et al., 2009; Gervilla et al., 2012; de Melo Portella et al., 2016; Arai et al., 2020; Grieco et al., 2020; Farré-de-Pablo et al., 2021).

In this study, we report the coexistence of both Al- and Cr-rich chromitites in the Gomati and sole Cr-rich chromitites in the Nea Roda ultramafic bodies. We provide new mineralogical and geochemical data and a revised view on the settings in which the chemically heterogenous podiform chromitites of east Chalkidiki were generated. After their formation, the host ultramafic occurrences underwent post-magmatic alteration. Using major and trace element chemistry of chromite and metasomatically affected minerals, we aim to decipher those processes. The combined results and interpretation on the Cr and platinum-group element (PGE) ore genesis and subsequent element remobilization due to alteration can serve as a case study for the modification of chromitite deposits throughout their life cycle and shed light into the geodynamic processes involved.

2 Regional geological settings

The Gomati and Nea Roda ultramafic bodies located in the east Chalkidiki peninsula (Figure 1A) represent rift-related Middle Triassic suites unit (Bonev et al., 2018) within the Vertiskos unit. This unit belongs to the SMM and consists of high-grade gneisses, schists and amphibolites with Neoproterozoic to Permian protoliths (Himmerkus et al., 2009), whereas marble occurs exclusively in the Kerdillion unit of the SMM, dated at 292.6 to 299.4 Ma (Himmerkus et al., 2012). Large bodies of Cenozoic granite intrude the SMM and partially the Gomati body (Siron et al., 2018 and references therein). The SMM is thought to represent an extension of the Rhodope Massif (Kydonakis et al., 2015), both containing meta-ophiolitic occurrences (Dixon and Dimitriadis, 1984; Bonev and Dilek, 2010b; González-Jiménez et al., 2015) with podiform chromitites in their mantle sections (Tarkian et al., 1991; Economou-Eliopoulos, 1996; Gervilla et al., 2012; González-Jiménez et al., 2015).

The Gomati suite consists of two highly serpentinized bodies, in contact with amphibolites (metagrabbros), metamorphosed at upper greenschist to lower amphibolitic conditions (Christodoulou and Hirst, 1985). The Gomati body is truncated by the 30.6 km NW-SE trending active Gomati-fault. Chromitites outcrop in both bodies. The most notable occurrences of the north domain include Agios Georgios, Frankokaliva, Moutsara, Paivouni and Tripes (Christodoulou,

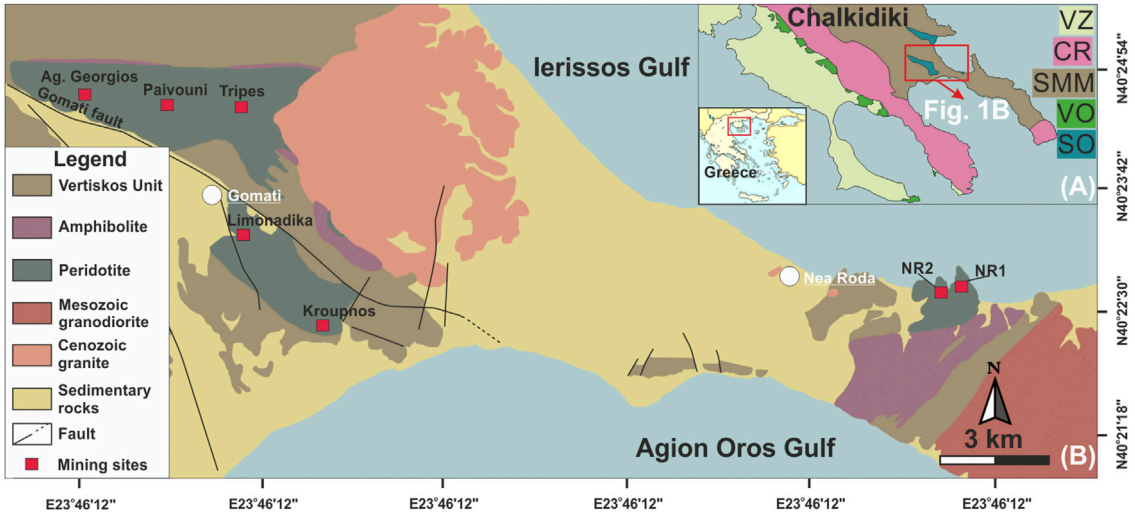

FIGURE 1
(A) Innermost Vardar ophiolites (VO) situated at the contact of the Vardar Zone (VZ), the Circum Rhodope belt (CR) and the Serbomacedonian Massif (SMM) hosted mafic-ultramafic magmatic suites (SO). **(B)** Simplified geological map of the studied ultramafic bodies, namely Gomati and Nea Roda (NR), modified after the Ierissos sheet of the Hellenic Survey of Geology and Mineral Exploration (HSGME). White circles represent the Gomati and Nea Roda villages.

1980). The south part includes the chromitite outcrops of Limonadika and Kroupnos (Figure 1B). The country rocks of the chromitites are harzburgite (Moutsara site), amphibolite and serpentinite (Paivouni and Tripes sites) (Christodoulou and Hirst, 1985). The chromitites' formation is attributed to alkali-rich melts deriving from a fertile mantle source (Christodoulou and Hirst, 1985). The NR suite consists of variably serpentinized dunite and harzburgite that underwent low greenschist facies metamorphism (Michailidis and Soldatos, 1995). Magnesite stockwork developed due to post-magmatic hydrothermal activity. Amphibolite and the metamorphic sequence of Vertiskos are in sharp contact with the NR ultramafic, SSZ-related body at the south; these rock formations have been overthrusted upon granodiorite. The chromitite occurrences are richer in Cr than the Gomati ones and compositionally comparable to the Vardar occurrences (e.g. Sideridis et al., 2018, Sideridis et al., 2021 and references therein; Figure 1B).

3 Materials and methods

3.1 Sample collection

Representative massive chromitite samples were collected from the Gomati and Nea Roda ultramafic bodies. More precisely, Al-rich massive chromitites from the Gomati (G1 chromitites) were collected from the mining sites of Paivouni and Tripes; Cr-rich massive chromitites from the Gomati (G2 chromitites) were collected from the mining sites Agios Georgios and Kroupnos; Massive and banded Cr-rich chromitites from the Nea Roda (NR chromitites) were collected from the sites NR1 and NR2, respectively. Serpentinites from the Gomati region were collected adjacent to the mining sites, whereas diopsidites were found penetrating the G1 chromitites from the Paivouni mining site. During fieldwork, criteria such as alteration degree, mode of occurrence, relationships with other lithologies and stratigraphical distribution were applied. More than fifty samples were collected around the area of seven abandoned mine sites.

3.2 Analytical methods

Electron microprobe analyses (EPMA) and electron back scattered images (B.S.I.) were carried out at the Eugen F. Stumpfl Laboratory of the Leoben University, Austria, using a Superpobe Jeol JXA 8200 (JEOL, Tokyo, Japan) instrument. Analyses of spinel and silicates were obtained in WDS mode, with an accelerating voltage of 15 kV and a beam current of 10 nA. The Kα lines were used in the analysis of Na, Mg, K, Al, Si, Ca, Ti, V, Cr, Zn, Mn, Fe and Ni, after instrument calibration on natural chromite, rhodonite, ilmenite, albite, pentlandite, wollastonite, kaersutite, sphalerite and metallic vanadium. The used diffracting crystals were: TAP for Na, Mg, Al; PETJ for K, Si, Ca; and LIFH for Ti, V, Cr, Zn, Mn, Fe, Ni. The counting times 20 and 10 s were used for peak and background, respectively, in the analysis of all major elements and were increased up to 60 and

30 s for the trace elements analyses. The following detection limits (in ppm) were automatically calculated by the microprobe software: Ca (50), Mg, K, Mn, Fe and Ni (100), Na, Al, V and Zn (150), Cr (200), Si and Ti (250). The amount of Fe^{3+} of chromite was calculated assuming the spinel stoichiometry $R^{2+}O\ R^{3+}_2O_3$.

The PGM and other accessory minerals were located *in situ* under reflect light microscope on polished chromitite sections, at 250–800 magnification. Grains smaller than 5 microns were only qualitatively analyzed by EDS. The quantitative composition of bigger grains was obtained in WDS mode, at a 20-kV accelerating voltage and 10-nA beam current, with a beam diameter of 1 μm. The counting times of peak and background were 15 and 5 s respectively. The Kα lines were used for S, As, Fe and Ni, Lα for Ir, Ru, Rh, Pd and Pt while Mα were used for Os. Synthetic pure metals, NiS, NiP and natural pyrite and niccolite were used as reference materials for the six PGE (Ru, Rh, Pd, Os, Ir, Pt), Ni, Fe, S, P and As respectively. The following diffracting crystals were selected: PETJ for S and P; PETH for Ru, Os and Rh; LIFH for Fe, Ni, Ir, Pt; and TAP for As. For interferences involving Ru-Rh and Rh-Pd the corrections were automatically performed. The detection limits are (in ppm): S, As and P (100), Fe, Ni and Cu (150), Ru, Rh and Pd (200), Os, Ir and Pt (800). Platinum concentrations were systematically below detection limit and have been removed from the analytical results.

Trace elements and REE contents in clinopyroxene and trace elements in spinel-group minerals were determined on polished thin sections by LA-ICP-MS (laser ablation inductively coupled plasma mass spectrometer) system at the NAWI Graz Central Lab for Water, Minerals and Rocks (University of Graz and Graz University of Technology), with an ESI New Wave 193 Excimer Laser (193 nm wavelength) coupled to a quadrupole Agilent 7500 CX mass spectrometer. A beam size of 50 μm, with a fluence of ~5 J/cm2, helium flow of 0.8 L/min, 25 s gas blank followed by 50 s of ablation and a dwell time of 20 s for each mass were used for the element analyses. The reference material NIST SRM 612 was used for standardization and Si and Al as internal calibration elements for diopside and spinel-group minerals, respectively. The USGS reference glass BCR-2G was analysed as monitor standard which could be reproduced within errors. For data reduction, the software "GLITTER" was used and the values for NIST SRM 612 were taken from Jochum et al. (2012).

Geochemical analyses of four serpentinite samples were performed at Activation Laboratories Ltd. Actlabs according to the packages of 4Lithores. This is a combination of packages 4B (lithium metaborate/tetraborate fusion ICP whole rock) and 4B2 (trace element ICP-MS). Geochemical analyses of PGE concentrations were performed at Activation Laboratories Ltd. Actlabs. Eleven chromitite samples were analyzed; three from G1 (GN1 - GN3), four from G2 (GS1 - GS4) and four from NR (NR1 - NR4) from seven mining sites (Figure 1). Aliquots of 25 g of sample were treated by the NiS fire assay procedure. The NiS beads were dissolved in concentrated HCl, and the PGE + Au residue collected on a filter paper. The residue underwent two irradiations and three separate counting steps for the PGE and Au. The irradiation is induced with neutrons, and the resulted gamma radiation was measured by Instrumental Neutron Activation Analysis (INAA). The detection limits (ppb) were: Os (2), Ir (0.1), Ru (5), Rh (0.2), Pt (5), Pd (2) and Au (0.5).

A Ni fragment enriched in P was extracted and investigated by X-ray diffraction at the university of Florence, Italy, using the procedure described by Zaccarini et al. (2019). Massive chromitites were processed in SGS Mineral Services, Canada, for recovery of heavy minerals, following the procedure described by Sideridis et al. (2018).

4 Results

4.1 Field relationships and petrographic study of chromitites

4.1.1 The Gomati chromitites

Both Gomati occurrences predominantly comprise schistose serpentinite displaying mesh and hour-glass texture (Figures 2A, B). Chromitites are divided into Al- (G1 chromitite: Tripes and Paivouni sites) and Cr-rich (G2 chromitite: Kroupnos and Ag. Georgios sites). Chromitite pods in all cases display: 1) sharp contacts with their host rocks (Figure 2C), 2) high degrees of alteration and 3) massive (Figure 2C), banded, schlieren and disseminated textures. The host rock of the Gomati chromitites, is composed of variably serpentinized dunite and bastitic serpentinite, whereas flaky serpentine and chlorite occur at their contact (Figure 2C). The G1 chromitites are often cross-cut by diopsidite forming pale-green veins with the paragenesis chlorite + diopside + titanite (Figure 2C). Chromitite in both sections of Gomati appears sheared and foliated (Figure 2D).

Both the G1 and G2 massive chromitite consists of interstitial lepidoblastic chlorite. Carbonates are either interstitial (Figure 2D) or fill veinlets accompanied with chlorite and locally with green-coloured garnet (Figure 2E). Garnet is developed within brecciated zones around chromite fragments in the case of G2 chromitites, whereas garnet within the G1 chromitites is amorphous and crystallized along fissures (Figure 2E). Diopside was identified as interstitial phase in the G1 chromitite (Figure 2F). The G1 spinel grains are coarse subrounded to subangular (up to 2,500 μm, avg. 550 μm) and in some cases, they appear elongated along the foliation plane (Figure 2D). They are further subdivided into a) homogenous spinel grains demonstrating mosaic-like texture (Figure 2G) and b) spinel grains with porous rims exhibiting strong ferrichromite alteration and intergrowth of chlorite, magnetite and minor sulphides, followed by altered inner rim around the pristine core (Figure 2H). The

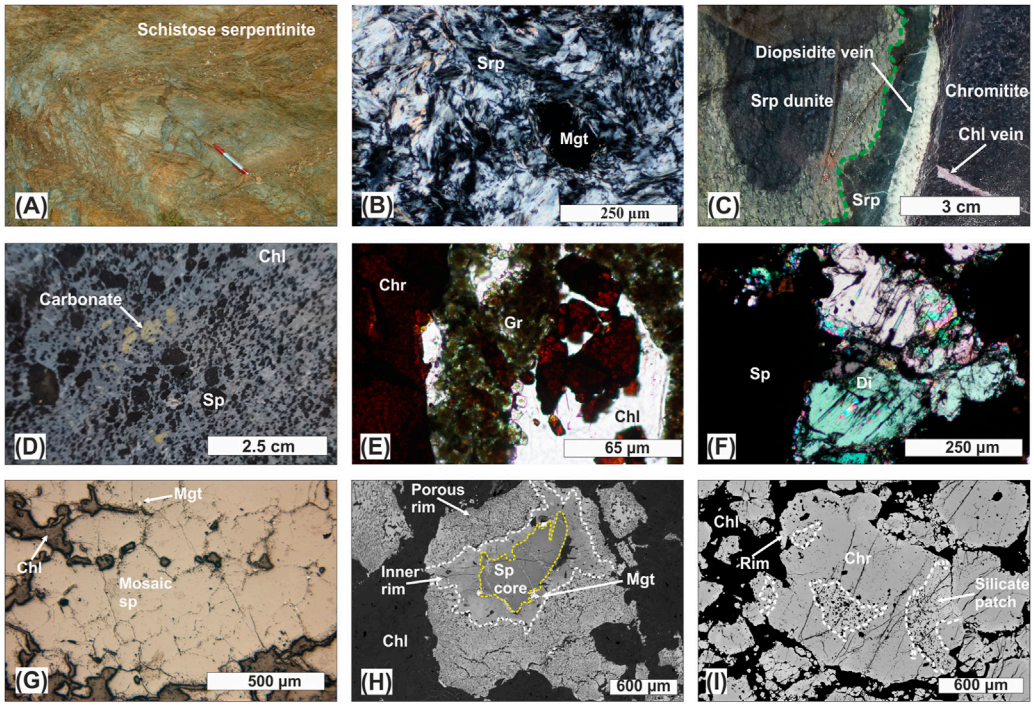

FIGURE 2
(A) Schistose serpentinite. **(B)** Photomicrograph of serpentinite comprised of flaky serpentine and magnetite. **(C)** Massive G1 chromitite cross-cut by chlorite veins. The host rock consists of serpentinized dunite and along the contact between the ore and the host flaky green-colored serpentine is developed along with a tectonized diopsidite vein consisting of titanite-diopside-chlorite. **(D)** Sheared and foliated disseminated chromitite from Gomati with dispersed carbonates. **(E)** Photomicrograph of shear zone filled with green-color garnet. **(F)** Photomicrograph of G1 chromitite composed of diopside interstices with spinel inclusions. **(G)** Photomicrograph of mosaic textured spinel (G1 chromitite). **(H)** B.S.I. of altered spinel grain (G1 chromitite) consisting of an outer porous rim followed by solid inner rim and dark colored pristine core. Cracks are filled with magnetite **(I)** B.S.I. of chromite (G2 chromitite) with thin alteration rim and chlorite patches developing irregularly. Abbreviations: Srp = serpentine; Chl = chlorite; Sp=spinel; Chr = chromite; Mgt = magnetite; Gr = Garnet; Ps = pseudomorph; Di = diopside; B.S.I. = Backscattered-electron image.

G2 chromite grains appear subrounded and subangular with low degree of alteration, commonly presenting chlorite intergrowths around the rims or/and in the form of patches within the chromite grains (Figure 2I).

4.1.2 The Nea Roda chromitites

The NR ultramafic body is composed mainly of altered harzburgite (Figure 3A). Chromitites are enveloped by variably serpentinized and carbonatized dunite bodies (Figure 3B). The host mantle section is listwaenitized and cross-cut by a magnesite stockwork. The massive NR chromitite (NR1 site; Figure 1B) contains the highest chromite (mineral chemistry analysed in section 4.2.1) concentrations (>90%; Figure 3C) and have not been affected by any prominent foliation and alteration (Figures 3C, D). Chlorite and few relic olivine grains exist within the chromite interstices (Figures 3E, F). Subangular chromite grains (up to 1,000 μm) appear moderately altered into ferrous chromite with prominent cataclastic and pull-apart textures. Carbonates, represented mainly by dolomite, are common in massive chromitite interstices and especially in the dunite envelopes (Figure 3F).

4.2 Mineral chemistry

4.2.1 Spinel-group minerals

The major, minor and trace element analyses of spinel-group minerals were conducted in the cores of the grains and along traverses as well. The EPMA and LA-ICP-MS analyses are reported in the Supplementary Tables S1 and S2, respectively.

Gomati section hosts two types of chromitites, Al-rich and Cr-rich. Their analyzed spinel-group mineral grains are classified as a) spinel and magnesiochromite (G1 chromitite) and b) chromite and magnesiochromite (G2 chromitite), the nomenclature is after Bosi et al. (2019). Cr# [Cr/(Cr + Al)] ranges between 0.48–0.67 (low-Cr) and 0.72–0.84 (high-Cr) and Mg# [Mg/(Mg + Fe^{2+})] between 0.48–0.73 and 0.41–0.60 for G1 and G2 chromitite hosted grains, respectively (Figure 4A). The G1 grains demonstrate variable and relatively high Al_2O_3 contents (18.04–27.40 wt%), whereas the G2 ones tend to be lower in Al_2O_3 (8.15–14.33 wt%). TiO_2 contents of the G1 (0.13–0.50 wt%) are slightly higher than those of the G2 (0.06–0.52 wt%) (Figure 4B). NR chromitites consist of

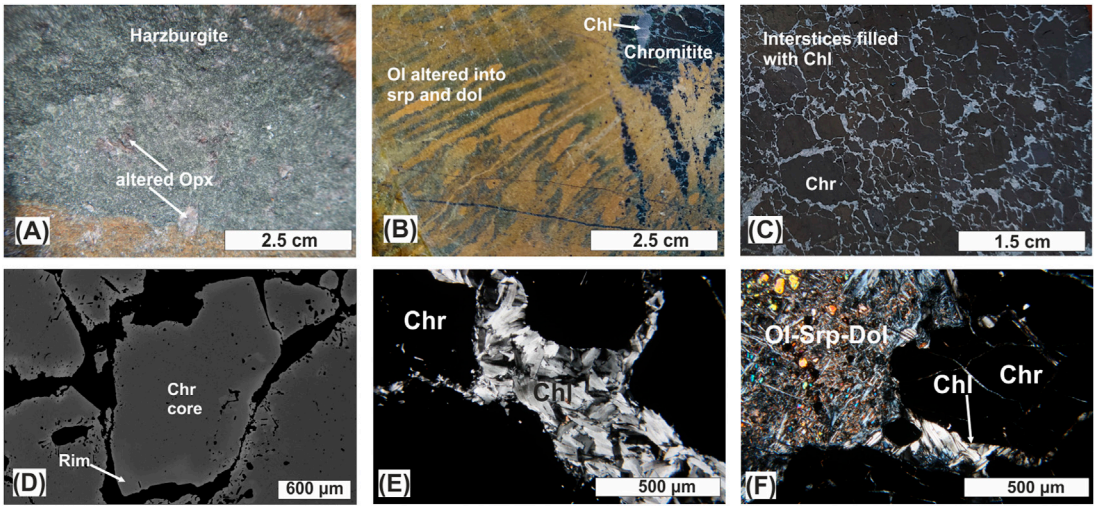

FIGURE 3
(A) Altered harzburgite of the NR mantle section. **(B)** Dunite envelope of NR chromitite, altered into dolomite and serpentine. **(C)** Cataclastic massive NR chromitite with interstices filled with chlorite. **(D)** B.S.I. of NR chromitite, note the evidently low degree of alteration of the chromite. **(E)** Photomicrograph of NR chromitite. **(F)** Photomicrograph of NR chromitite in contact with altered dunite. Abbreviations: Srp = serpentine; Chl = chlorite; Chr = chromite; Opx = orthopyroxene; Dol = dolomite; B.S.I. = Backscattered-electron image.

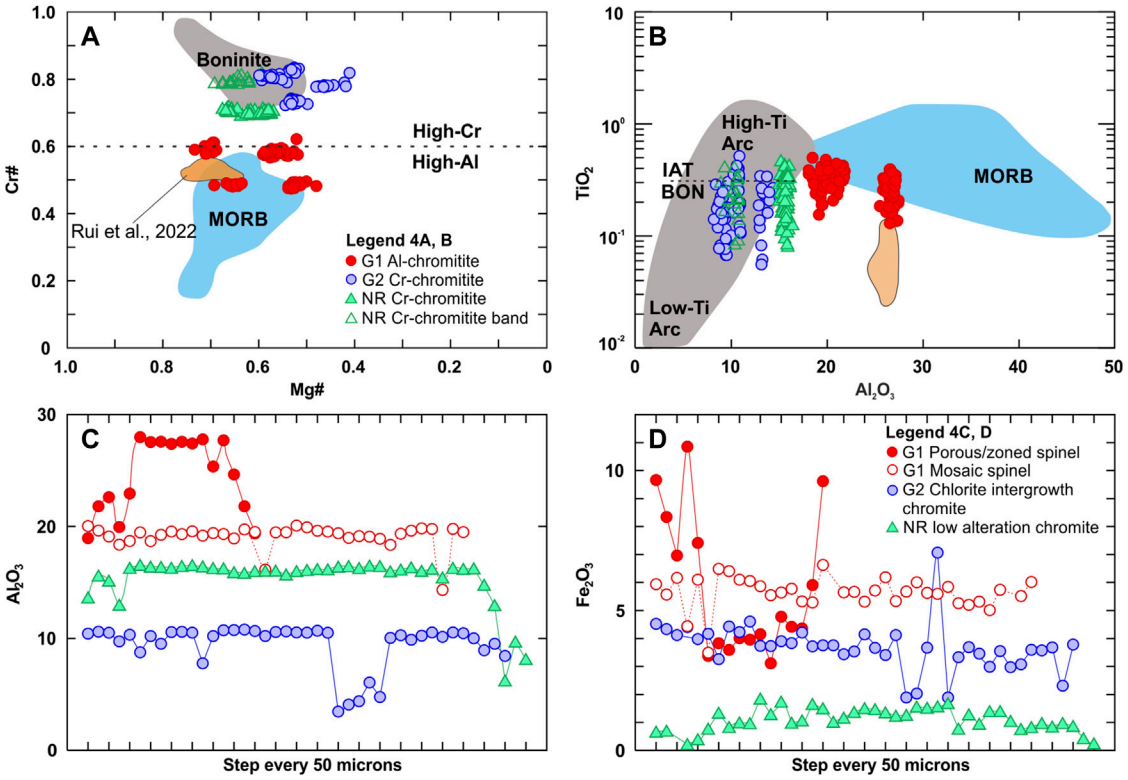

FIGURE 4
Plots of spinel core analyses from the studied chromitites: **(A)** Cr# *vs.* Mg#. **(B)** LogTiO_2 *vs.* Al_2O_3; Analyses conducted in traverses in texturally different grains. **(C)** Al_2O_3 distribution. **(D)** Fe_2O_3 distribution. Fields after Kamenetsky et al. (2001). Abbreviations: IAT = island arc tholeiites; BON = boninites; MORB = mid-ocean ridge basalts.

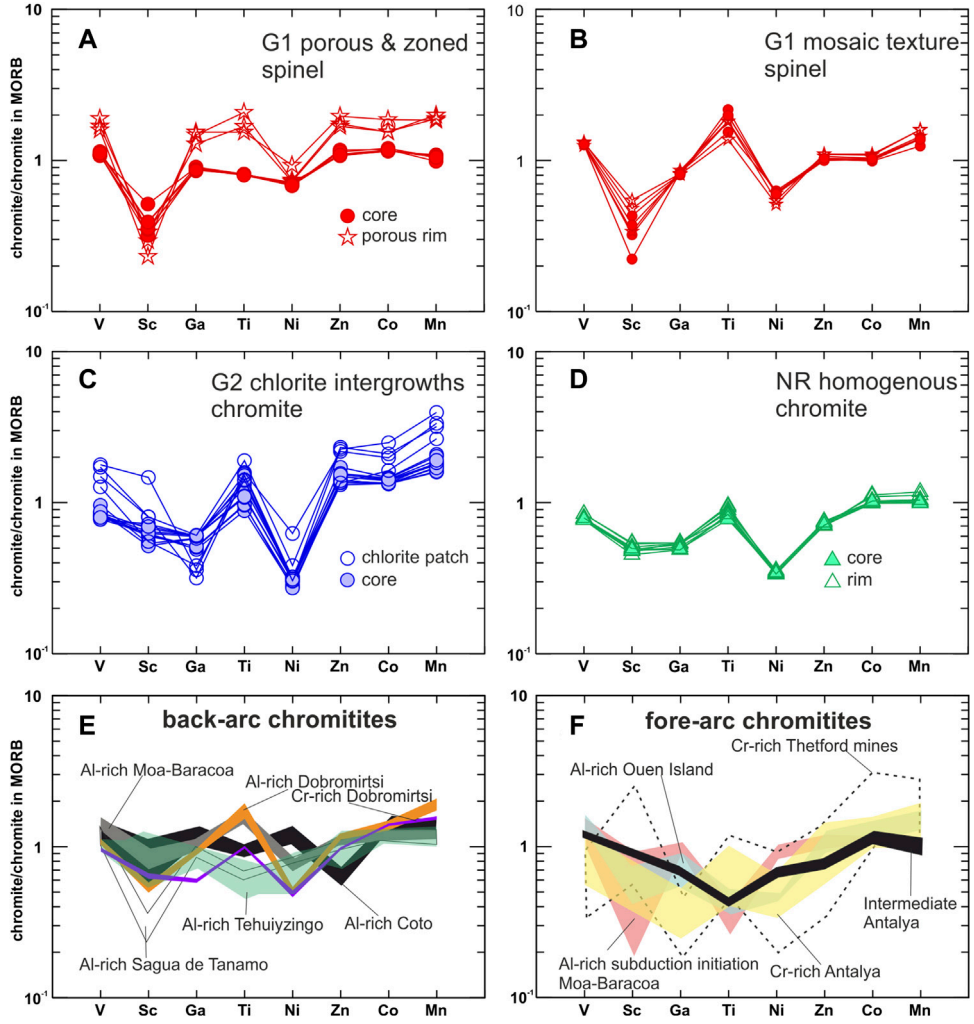

FIGURE 5
(A–D) MORB normalized patterns (after Pagé and Barnes, 2009) of LA-ICP-MS analyzed spinel-group mineral grains per texture; **(E)** compositional fields of back-arc chromitites: Al-rich Moa-Baracoa (Colás et al., 2014); Al-rich Sagua de Tanamo (González-Jiménez et al., 2015); Al-rich Tehuitzingo (Colás et al., 2019); Al-rich Coto (Yao, 1999); Al-rich Dobromirtsi and Cr-rich Dobromirtsi (González-Jiménez et al., 2015); **(F)** compositional fields of fore-arc chromitites: Al-rich Ouen Island (González-Jiménez et al., 2011); Al-rich Moa-Baracoa (subduction initiation) (Rui et al., 2022); intermediate and Cr-rich Antalya (Uysal et al., 2016); Cr-rich Thetford mines (Pagé and Barnes, 2009).

magnesiochromite (nomenclature after Bosi et al., 2019). Based on Cr# values, all the NR chromitites are classified as high-Cr, ranging from 0.69 to 0.82. The NR chromite grains are Ti-poor (0.08–0.46 wt%), demonstrating Al_2O_3 contents between 8.89 and 16.38 wt% and Mg# from 0.57 to 0.69. Compositionally, the NR massive chromitites are intermediate in composition between G1 and G2. For reasons of simplicity, the term 'spinel' will henceforth be used when referred to the G1, while the term "chromite" will refer to the G2 and NR chromitites. Traverses from core to rim (Figures 4C, D) of selected grains were conducted, focusing on the alteration textural features. Analyses near rims and cracks revealed an increase in Cr and Fe^{2+} with decrease in Al and Mg (Process 1; Figure 4C). Concerning textures with porous rims (G1 chromitites), a substantial increase of Fe^{3+} is also noted (Process 2; Figure 4D). The B.S.I. of the analyzed grains are presented in the Supplementary Figure S1.

Trace element MORB-normalized patterns (after Pagé and Barnes, 2009) of G1 cores are characterized by negative Sc and Ni anomalies with almost flat Ga-Mn patterns resembling MORB compositions. Porous rims show an enrichment in Ti and Ni-Mn (Figure 5A). G1 grains with mosaic-like texture exhibit no substantial chemical differences with respect to core-rim analyses (Figure 5B). The G2 core analyses demonstrate negative V-Ni patterns with positive Ti anomalies and elevated Zn-Mn concentrations up to twice the MORB

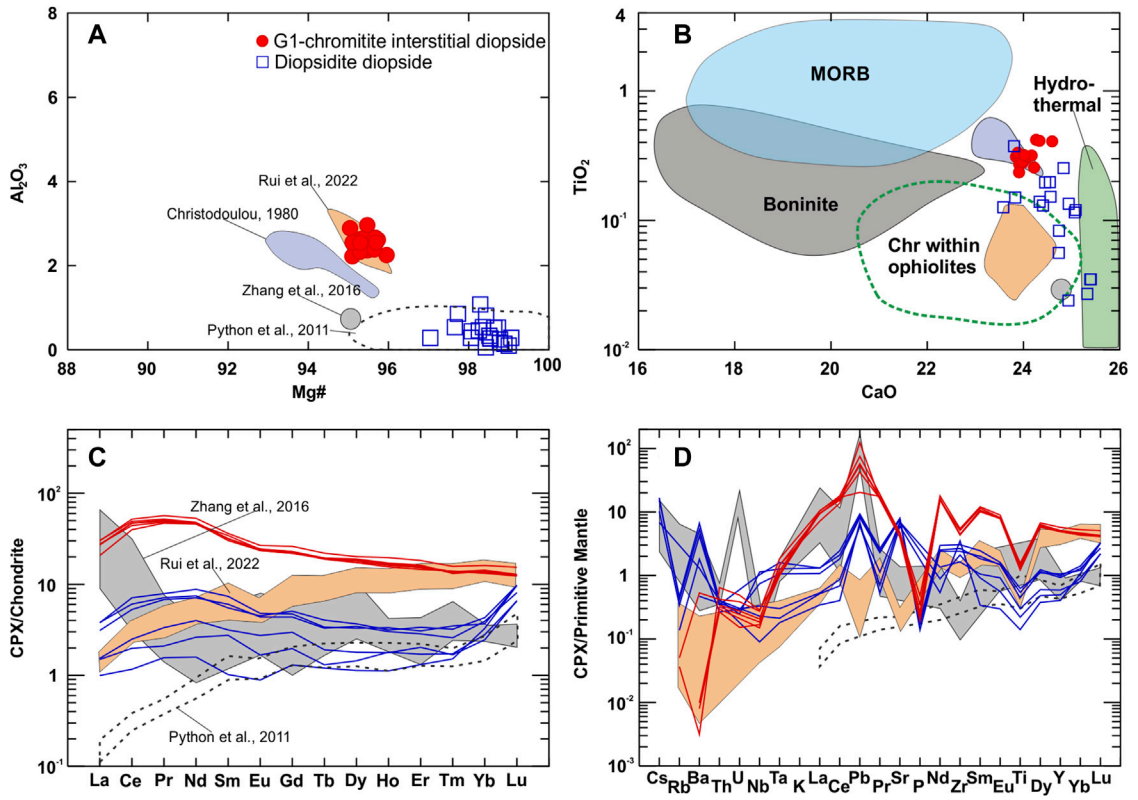

FIGURE 6
Diopside microprobe analyses per lithotype: **(A)** Al_2O_3 *vs* Mg# plot; **(B)** TiO_2 *vs* CaO plot. The dark-blue field consist of diopside inclusions in G1 chromitites, reported by Christodoulou (1980); the dotted line represents diopside analyses from Oman diopsidites (Python et al., 2011), orange field represents analyses of chromitite hosted diopside of Moa-Baracoa (Rui et al., 2022) and gray field represents analyses of chromitite hosted diopside of Kop Ophiolite (Zhang et al., 2016). Fields of MORB (blue), boninite (grey), hydrothermal (green) and clinopyroxene associated with chromite in ophiolitic rocks (dotted green line, Chr within ophiolites) are from Su et al. (2021) and references therein. Chondrite and Primitive mantle-normalized (PM_N) LA-ICP-MS analyses of clinopyroxenes' (CPX) trace elements plots **(C, D)** after Sun and McDonough (1989).

composition (Figure 5C). The alteration noticed in the rim analyses in this case is marked by increased Zn-Mn contents. NR core-rim analyses demonstrate almost identical patterns, with MORB-like V, Ti, Co and Mn and relatively depleted Sc to Ga and Ni to Zn concentrations (Figure 5D). In all studied spinel-group minerals, rim analyses neighboring directly with other spinel grains, rather than with interstitial chlorite, do not demonstrate substantial major and trace element variability.

4.2.2 Silicates

Clinopyroxene, classified as diopside according to the nomenclature of Morimoto (1988) occurs only in the G1 chromitite, both as an interstitial component as well as within secondary diopsidite veins along with chlorite and titanite. The interstitial diopside displays relatively high amounts of Al_2O_3 (2.22–2.96 wt%), Cr_2O_3 (0.96–1.18 wt%) and TiO_2 (0.24–0.42 wt%) compared to the vein variety (0.06–1.08, <0.82 and 0.04–0.37 wt% respectively) (Figures 6A, B; EMPA analyses: Supplementary Table S3). Microanalyses of diopside inclusions within spinel grains reported by Christodoulou (1980) are presented for comparison and they are chemically similar to the diopside in the G1 chromitite. Chondrite-normalized REE patterns of both diopside types display strong similarities to each other (LA-ICP-MS analyses: Supplementary Table S4), described by convex upward LREE and slightly negative Nd-Tm slopes (Figure 6C). The heavy REE, Yb and Lu differ in slope and show an increase in clinopyroxenes from the diopsidite, resulting in a sinusoidal REE pattern (Figure 6C). Diopside hosted within the G1-chromitite is more enriched in ΣREE. In the primitive mantle normalized plot (Figure 6D) HFSE (High Field Strength elements) are found in higher concentrations in the chromitite hosted diopside, whereas LILE (Large-Ion Lithophile Elements: Li, Be, B, Ba, Sr) are enriched in the diopsidite variety. More precisely, the diopsidite variety is 8–11, 12–22 and 14–39 times more enriched than PM values for Li, Be and B, respectively. The G1-chromitite hosted variety is 5–7, 9–13 and 1–2 times more enriched than PM for Li, Be and B, respectively. Negative Ti, Nb and P and positive

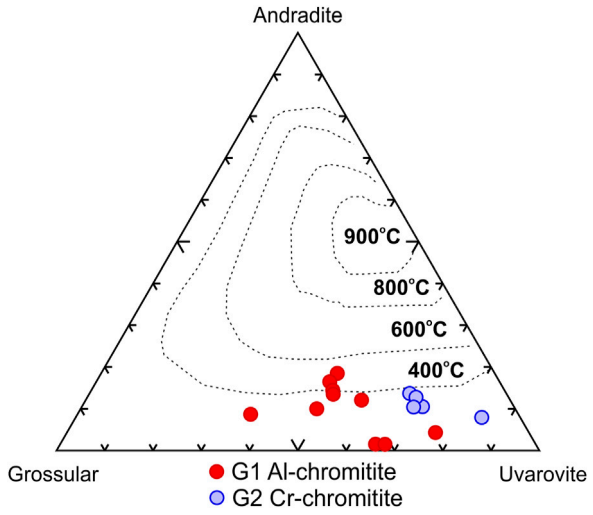

FIGURE 7
Ternary diagram of garnet hosted in G1 and G2 chromitites, in the grossular-uvarovite-andradite system. Dotted lines represent the stability limits of the aforementioned solid solution, after Melcher et al. (1997) and references therein.

Pb anomalies are present in both types (Figure 6D). The usually constant HFSE ratio Zr/Hf (36.25 for primitive mantle (PM) and 36.10 for normal mid-ocean ridge basalt (NMORB) (Sun and McDonough, 1989) is different in both clinopyroxene occurrences. The Zr/Hf ratio differs significantly from the PM and NMORB ratio in the diopsidite (15.90–17.44), however it is slightly variable but consistent with PM and NMORB in the chromitite hosted diopside (31.52–38.31). However, the Y/Dy ratio (6.17 and 6.15 for PM and NMORB, respectively) is comparable to PM and NMORB, ranging between 5.00–6.63 and 5.00–5.28 for the diopsidite and chromitite respectively.

Chlorite has been identified in all chromitites of this study. According to the nomenclature of Hey (1954) they are classified as penninite and clinochlore (Supplementary Figure S2). Chlorite in the G1 chromitite is slightly enriched in FeO (0.79–3.11 wt%), followed by the NR (0.68–1.38 wt%) and G2 chlorites (0.68–1.30 wt%). The Cr_2O_3 contents are generally high; G1 chlorite analyses range between 0.03–4.87 wt%, G2 4.26–5.82 wt% and NR 1.58–4.67 wt% (Supplementary Table S5). Chlorite in contact with garnet, diopside or PGM does not demonstrate any noticeable chemical difference compared to its interstitial counterpart.

Garnet grains from the G1 chromitite are dominated by uvarovite and grossular molecule having an average composition of $Adr_{0.09}Grs_{0.35}Uv_{0.55}$ with TiO_2 contents ranging from 1.01 to 2.12 wt%. The garnet occurring in the G2 chromitite is rich in uvarovite endmember showing an average composition of $Adr_{0.11}Grs_{0.17}Uv_{0.72}$ and poorer in TiO_2 (0.20–0.73 wt%) (Figure 7; Supplementary Table S6). No compositional zoning has been observed. Titanite from the diopsidite veins demonstrate low Fe (<0.009 apfu) and Al (<0.096 apfu) contents (Supplementary Figure S3). TiO_2 ranges between 34.90–40.62 wt% and Cr_2O_3 ranges between 0.01–1.21 (Supplementary Table S7).

4.2.3 PGM and other metal phases within chromitites

PGM appear either as inclusions in spinel-group minerals or within interstitial chlorite in the G2 and NR chromitites (PGM were rare in G1 chromitites). Texturally and chemically, PGM are distinguished into 1) euhedral to subhedral laurite inclusions in chromite ranging between 7–10 μm (Figure 8A), 2) subrounded PGM grains (platarsite, ruarsite) ~10 μm within the interstitial matrix or the rims of spinel (Figures 8B, C) and 3) minute irarsite and sperrylite (<5 μm) in contact with laurite (Figures 8C–E). Other minute phases include pentlandite (Figure 8D), Ni-Ir-S and Ni-sulfides (Figure 8F). Apart from the aforementioned PGM, phases rich in Sb have been identified in the Gomati body and particularly either as Ni-Sb or as PGM Pd,Cu,Ni-Sb (Figures 8G, H). A ~ 20 μm grain of Ni enriched in P content, $(Ni,Fe)_5P$, yellow in color and isotropic under a reflected-light microscope, was found in a crack filled with chlorite within the NR chromitite (Figure 8I).

Laurite grains from the NR and G2 chromitites contain relatively high amounts of arsenic 1.60–3.29 and 0.54–0.58 wt%, respectively. Os (G2 = 12.03–12.32 wt% and NR = 6.48–14.45 wt%) and Ir (G2= 6.66–6.97 wt% and NR= 2.56–8.28 wt%) substitute for Ru, which ranges between 42.62–44.26 wt% and 38.93–48.78 wt% in the laurite grains of the G2 and NR chromitites, respectively. A few laurite grains in the NR chromitite demonstrate oscillatory zoning (Figure 8E), whereas the G2 counterparts display desulfurized Ru rims (Figure 8A). Platarsite found in the chlorite interstices of NR is in contact with sperrylite and contains small amounts of iridium-PGE (IPGE; Os < 0.46 wt%, Ir = 4.99–5.00 wt% and Ru = 13.44–13.94 wt%). Platinum ranges between 30.04 and 30.60 wt% followed by Rh and Pd, 3.84–4.03 and 1.20–1.36 wt%, respectively. Sulfur in platarsite ranges from 12.76 to 13.13 wt%, whereas arsenic ranges between 30.03 and 31.49 wt%. Ruarsite in the G2 chromitite, located at spinel rims, contains Ru 28.84–28.97 and Os 21.03–22.01 wt%, whereas As and S contents range between 31.86–32.14 and 13.29–13.36 wt% respectively. Irarsite grains were found in both the G2 and NR chromitites. The analyzed PGM are presented in Figure 9 and Supplementary Table S8.

4.3 Chromitite PGE and serpentinite whole-rock geochemistry

PGE concentrations from eleven massive chromitites were examined and the results are presented in Supplementary Table S9. The G1 chromitites display the

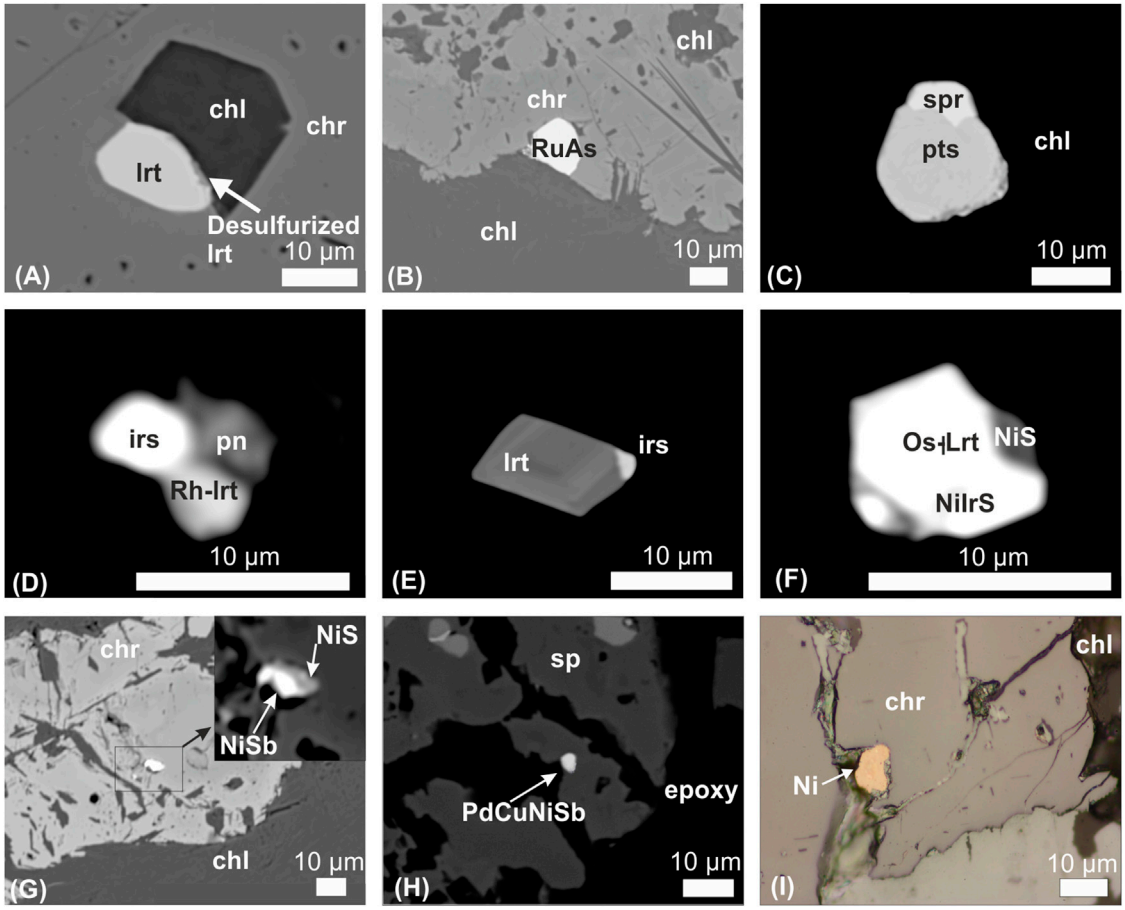

FIGURE 8
B.S.I. of PGM and related phases, the white bar is 10 μm in length: **(A)** subhedral G2 laurite grain in contact with chlorite and desulfurized laurite as inclusions within spinel. **(B)** G2 subrounded ruarsite engulfed within the spinel rim, primary minerals have been altered into chlorite. **(C)** NR subrounded platarsite in contact with anhedral sperrylite within the chlorite interstices. **(D)** NR PGM assemblage composed of subhedral Rh-rich laurite, irarsite and anhedral pentlandite in contact with chlorite **(E)** NR oscillatory laurite in contact with irarsite and chlorite. **(F)** NR Os-rich subhedral laurite in contact with Ni-"iridsite" and Ni-sulfide. **(G)** G2 Ni-antimonide and Ni-sulfide within altered spinel with chlorite intergrowths. **(H)** G1 PGM PdCuNiSb enclosed in liberated spinel grain from chromitite concentrates. **(I)** Photomicrograph of NR Ni enriched in P along the contact of spinel and chlorite. Abbreviations: Lrt = laurite, Chl = chlorite, Chr = chromite, Sp = spinel; RuAs = ruarsite, Irs = irarsite, Pn = pentlandite, NiS = Ni-sulfide, NiSb = Ni-antimonide, NiS = Ni-sulfide and Ni = Ni enriched in P.

lowest ΣPGE (45.4–135.6 ppb, avg.= 83.5 ppb), characterized by elevated palladium-PGE (PPGE) concentrations (Avg. PPGE/IPGE = 0.93) and Pd/Ir ratios (1.14–5.53;). Their normalized PGE patterns demonstrate positive Ru anomalies and depleted Ru-Pt profiles, with a slight enrichment in Pd (Figures 10A, B). The G2 chromitites are more enriched in ΣPGE (64.3–264.8 ppb, avg. = 135.7 ppb), described by lower PPGE concentrations (Avg. PPGE/IPGE = 0.31) and low Pd/Ir ratios (0.14–0.22) with the exception of a single sample with Pd/Ir = 7.69. Their normalized PGE patterns are closely comparable to those of G1, albeit exhibiting more prominent positive Ru anomalies and pronounce negative Ru - Pt slopes, with a slight increase in Pd. The normalized PGE patterns of NR chromitites greatly resemble the G2 counterparts. Their ΣPGE (132.0–199.0 ppb, avg.= 169.3 ppb) are slightly higher in concentration than in the G2 samples, displaying enrichment in IPGE concentrations (Avg. PPGE/IPGE = 0.17 and Pd/Ir = 0.20–0.41).

The serpentinites display MgO/SiO_2 and Al_2O_3/SiO_2 ratios ranging between 0.83–0.88 and 0.01–0.06, respectively, exhibiting enrichments in arsenic and antimony when compared to PM values, 16–19 and 2.1–2.8 ppm, respectively (Figure 11). Fluid-mobile-elements (FME) such as Cs, U and Ba display values of <0.5, 0.03–0.94 and 5–12 ppm, respectively. LREE demonstrate enrichment relative to the flat MREE and HREE patterns, whereas Nb-Ta, Zr and Ti are depleted if

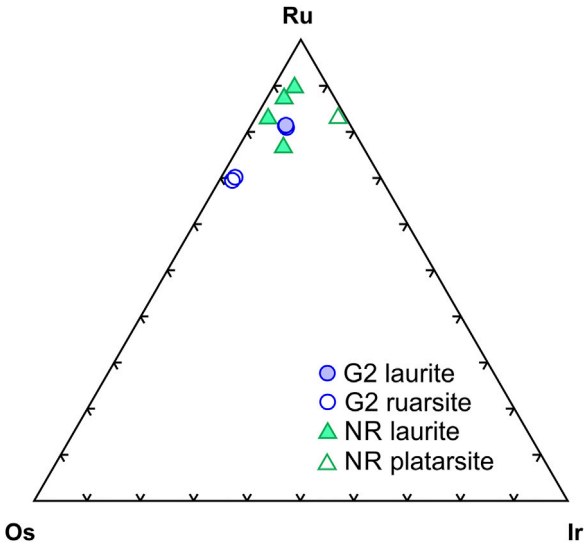

FIGURE 9
Ternary diagram of PGM analyses; open symbols represent secondary PGM, whereas full symbols represent primary PGM.

compared to the PM (0.5*PM). These rocks are rich in Ni (1,620–2,540 ppm) and Cr (2,640–10,000 ppm) consistent with their refractory mantle origin. The whole-rock geochemical analyses are presented in the Supplementary Table S10.

5 Discussion

5.1 Identification of pristine spinel compositions and affinities

Major and trace elements in spinel-group minerals within chromitites are commonly used to estimate their parental melt composition and classify them according to their normalized patterns, respectively. Both approaches have been implemented upon metamorphosed chromitites (González-Jiménez et al., 2015; Colás et al., 2019). This is achieved by careful examination of chemical changes in core and rims of the analyzed grains. In the present study, individual grains from G1, G2 and NR chromitites have been analyzed *via* EPMA and LA-ICP-MS to test this theory.

Concerning the G1 chromitite bodies, two cases were encountered and examined: 1) chromitites comprised of zoned spinel grains with porous rims demonstrating significant trace element variations from core to rim with increase of Zn-Co-Mn, in short ZCM, (on average, from core 1,636 to rim 2,633 ppm) and Ti coupled with a decrease in Sc (Figure 5A) and 2) chromitites comprised of mosaic-like texture spinel grains with homogenous normalized patterns characterized by positive Ti and negative Sc anomalies (Figure 5B). Based on these, it is considered that increase in ZCM + Ti and decrease in Sc (coupled with decrease in Al_2O_3 and increase in $Fe^{3+}\# = Fe^{3+}/\Sigma Fe$) are traits related to alteration (González-Jiménez et al., 2015; Colás et al., 2019). Hence the pristine patterns of G1 ought

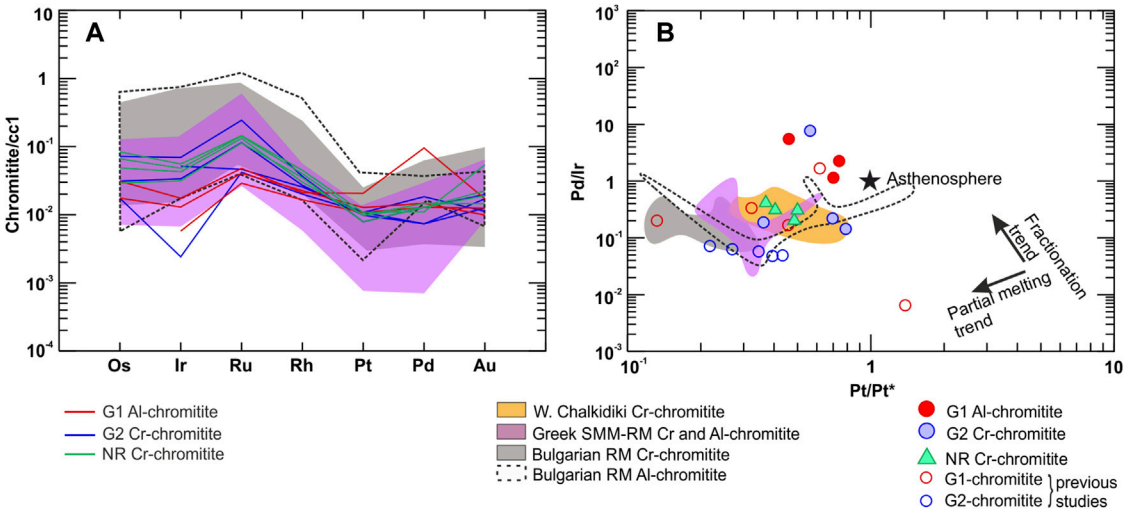

FIGURE 10
(A) Chondrite normalized PGE patterns of the Gomati and Nea Roda chromitites, CC1 Values after Naldrett and Duke (1980) **(B)** Pd/Ir *vs.* Pt/Pt* = $Pt_N/(Rh_N \times Pd_N)^{1/2}$ plot of the studied chromitites (after Garuti et al., 1997). Purple field after Economou-Eliopoulos (1996) and references therein; gray field after Tarkian et al. (1991) and González-Jiménez et al. (2015); dotted line field after González-Jiménez et al. (2015); orange field after Economou-Eliopoulos (1996) and Sideridis et al. (2021); G1 and G2 chromitite from previous studies are after Economou-Eliopoulos (1996) and Bussolesi et al. (2022b).

to be flat (MORB-level) with negative Sc and weak negative Ni anomalies. Such patterns are typical of high-Al (Zhou et al., 2014) and more precisely, of back-arc Al-chromitites of Coto, Tehuitzingo, Moa-Baracoa, Sagua de Tanamo and Dobromitsi (Yao, 1999; González-Jiménez et al., 2011, González-Jiménez et al., 2015; Colás et al., 2014, Colás et al., 2019 and references therein; Figure 5E). Concerning the mosaic textured case, most likely, represents a product of complete re-equilibration as its annealing texture suggests. The pristine G1 spinel normalized patterns are also comparable with fore-arc chromitites (Figure 5F) such as: a) the case of Al-rich, subduction initiation Moa-Baracoa chromitites reported by Rui et al. (2022) though in this occurrence prominent negative Ti anomalies are noted and b) Ouen Island (González-Jiménez et al., 2011).

Regarding the G2 grains, two cases were encountered and examined: a) grains with low degree of alteration and chlorite intergrowths as confined altered zones, with an increase in ZCM being noted in the latter (on average, from core 2,500 to rim 4,175 ppm; Figure 5C), and b) grains with low-alteration degrees and little chemical variation in trace elements and a small increase around the crystal rims. Since the core analyses have low ZCM concentrations and they are free of chlorite inclusions, they represent pristine composition. The similarities of the normalized trace element patterns with other pristine chromite grains from Cr-rich fore-arc chromitites of Antalya and Thetford mines (Pagé and Barnes, 2009; Zhou et al., 2014; González-Jiménez et al., 2015; Akbulut et al., 2016; Figure 5F), are also in favor of the core analyses representing pristine compositions. The normalized patterns are characterized by mildly negative V-Ga patterns, positive Ti and negative Ni anomalies and almost flat Zn-Mn patterns. However, similar patterns are also consistent with back-arc Al- and Cr-chromitites of Dobromirtsi and Al-chromitites of Moa-Baracoa (Colás et al., 2014).

The seemingly unaltered NR grains present no trace element chemical variation from core to rim (Figure 5D). Since these chromitites were most-likely re-equilibrated (Bussolesi et al., 2022a), it can be assumed that their patterns depict this effect and therefore not primary compositions. Despite the above, it is generally considered that chromitites with high spinel/silicate ratios are only slightly affected by post-magmatic processes (e.g. González-Jiménez et al., 2015; Akbulut et al., 2022), this is why although NR are re-equilibrated their chromite major composition must have not been significantly altered. The normalized patterns of the studied grains demonstrate characteristics that are intermediate between the G1 and G2, with weak negative Sc, positive Ti and pronounced negative Ni anomaly. These patterns are also reminiscent of Cr-rich chromitites and are almost identical to those of Bulgarian Al-rich chromitites reported by Colás et al. (2014).

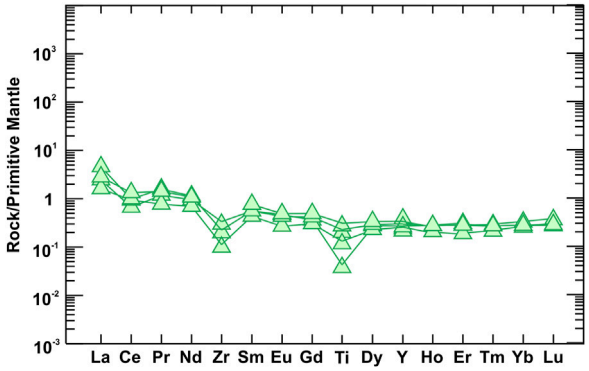

FIGURE 11
PM_N (Sun and McDonough, 1989) trace element patterns of Gomati serpentinites.

In all studied cases, the non-primary spinel-group analyses are enriched in ZCM + Ti and this has been previously reported for metamorphic spinels (González-Jiménez et al., 2015 and references therein). PGM enclosed in metamorphic chromite of this study are also affected; laurite enclosed in chromite of the NR chromitite appears compositionally modified whereas laurite in pristine chromite of the G2 chromitite represents primary compositions (see section 5.4). Hence, whereas Ti contents in NR are not considered primary, Ti in unaltered cores of Gomati is taken to depict primary compositions and this also applies to other metamorphosed chromitites (Colás et al., 2019). Non-stoichiometric spinel has been previously reported by researchers (Rollinson and Adetunji, 2013; Lenaz et al., 2014). Despite the chemical changes reported in this study and based on the methodology used, the spinel-group minerals are stoichiometric, and this is the case for other metamorphosed occurrences (Lenaz et al., 2018).

5.2 Parental melts and geotectonic settings of bimodal chromitites

Many studies argue for the connection of chromite composition, within massive chromitites, and the parental melts thereof. Equations to calculate the Al_2O_3 and TiO_2 of the parental melts were proposed by Rollinson (2008) based on previous work done by Kamenetsky et al. (2001) (Eqs. 1–4).

Equations for high-Cr chromitite:

$$Al_2O_{3melt} = 5.2182 \times \ln Al_2O_{3chromite} - 1.0505 \quad (1)$$

$$TiO_{2melt} = 1.0963 \times TiO_{2chromite} 0.7863 \quad (2)$$

Equations for high-Al chromitite:

$$Al_2O_{3melt} = 7.1518 \times Al_2O_{3chromite} 0.2387 \quad (3)$$

$$TiO_{2melt} = 1.5907 \times TiO_{2chromite} 0.6322 \quad (4)$$

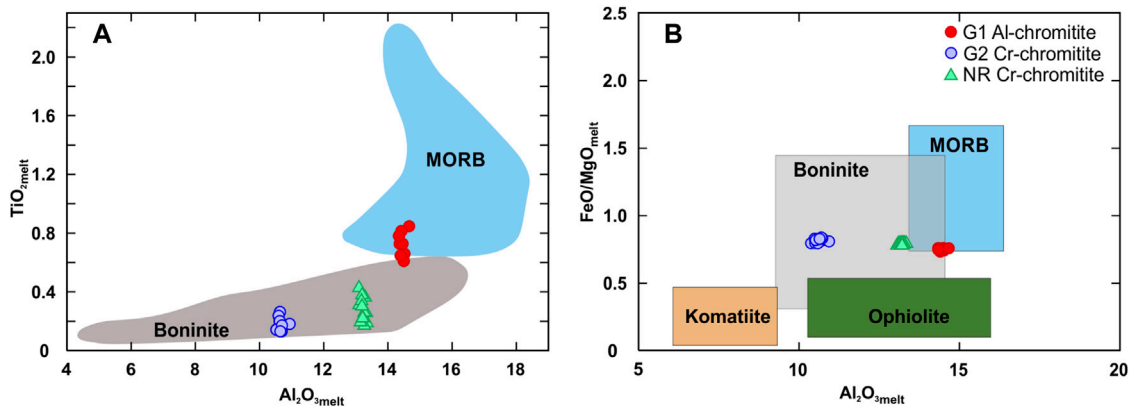

FIGURE 12
Calculated chromitite parental melt compositions **(A)** Al_2O_3 *vs.* TiO_2 (fields of MORB: le Roex et al. (1987) and fields of Boninite: Kamenetsky et al. (2001) and references therein and **(B)** FeO/MgO vs. Al_2O_3, fields are after Barnes and Roeder (2001).

Maurel (1984) on the other hand, proposed Eq. 5 in order to determine FeO/MgO_{melt} ratios, where $Al\#_{chromite} = Al/(Al+Cr+Fe^{3+})$ and $Fe^{3+}\#_{chromite}=Fe^{3+}/(Al+Cr+Fe^{3+})$.

$$\ln(FeO/MgO)_{chromite} = 0.47 - 1.07Al\#_{chromite} + 0.64Fe^{3+}\#_{chromite} + \ln(FeO/MgO)_{melt} \quad (5)$$

The most primitive compositions from the cores of spinel-group minerals of massive chromitites were used for the calculations. The parental melts of G1 are richer in Al_2O_3 (14.34–14.51 wt%), followed by NR (13.06–13.35 wt%) and lastly G2 (10.49–10.94 wt%) (Figure 12A). The concentration of TiO_{2melt} is comparably low in the cases of G2 with values lower than 0.26 wt%. The G1 records a slight enrichment in TiO_{2melt} (0.61–0.81 wt%) (Figure 12A), the same concentrations, although calculated for the NR, should be taken with caution, since Ti was re-mobilized (see section 5.1). The FeO/MgO_{melt} ratios for the G1, NR and G2 chromitites range between 0.73–0.76, 0.77–0.79 and 0.79–0.83 wt% respectively (Figure 12B). These ratios are generally consistent for all chromitite types. The composition of the G1 parental melts is akin to a MORB source (Melcher et al., 1997; Rollinson, 2008; Zaccarini et al., 2011; Chen et al., 2019), while the G2 and NR parental melts demonstrate boninitic affinities (Falloon et al., 2008; Koutsovitis and Magganas, 2016; Chen et al., 2019; Huang et al., 2021).

G1 chromitites consist of spinels resembling those in equilibrium with MORB lavas (Figures 4A, B). On the contrary, the G2 and NR chromite analyses compare well with spinel hosted within boninitic lavas (Figures 4A, B). Coexistence of Al- and Cr-rich chromitites in such proximity and without any fault bringing together two separate sections has been interpreted in the following ways: 1) evolution of a single initially Cr-rich batch magma of boninitic affinity into Al-enriched magma residue (Zaccarini et al., 2011; Uysal et al., 2016), 2) subduction initiation starting with formation of Al-rich chromitites after MORB-like melts produced in fore-arc spreading followed by Cr-rich varieties with progressive arc maturation and production of transitional and boninitic melts (Rollinson and Adetunji, 2013; Xiong et al., 2017; Rui et al., 2022) and 3) generation of Al-rich chromitites in either MOR or back-arc settings and subsequent transition into a SSZ (Rollinson, 2008; Uysal et al., 2009; González-Jiménez et al., 2011). Generation of the bimodal chromitites of the RM in a back-arc has been proposed (González-Jiménez et al., 2015).

5.3 Geothermometry estimations based on silicate chemistry and spinel trace element abundances

Four empirical chlorite geothermometers were applied in the studied chromitites (Cathelineau and Nieva, 1985; Kranidiotis and MacLean, 1987; Cathelineau, 1988; Zang and Fyfe, 1995). The temperature dependance in chlorite is controlled by the Al substitution over Si in the tetrahedral site (Cathelineau and Nieva, 1985). The temperatures (°C) calculated for the chlorites in the G1, G2 and NR chromitites are presented in Table 1.

These temperature results are generally consistent between the three domains. Consequently, the studied ultramafic bodies must have undergone similar post-magmatic effects that point to a lower-greenschist facies overprint; similar conditions have been reported from metamorphic rocks within the SMM and the RM (Kydonakis et al., 2015). Moreover, chlorite in contact with PGM grains or included in spinel grain displays insignificant temperature differences compared to chlorite hosted within

TABLE 1 Chlorite temperature calculations (°C) based on four different geothermometers.

Chlorite geothermometer in Celsius degrees				
Chromitite	Cathelineau and Nieva, (1985)	Kranidiotis and MacLean, (1987)	Cathelineau (1988)	Zang and Fyfe, (1995)
G1	170–276	171–277	169–330	200–306
G2	164–203	165–204	160–219	220–245
NR	171–244	172–246	171–282	202–275

the chromitite interstices. Grossular–andradite–uvarovite garnet is a mineral phase that can form under a variety of conditions, ranging from low-grade metasomatic processes to local regional metamorphism. Temperature estimations of the two garnet groups yielded values ≤400°C for the G1 and <500°C for the G2 counterparts, which typically falls under the temperature range of greenschist facies.

Colás et al. (2019) provided insights regarding the thermal control of the ZCM enrichments in metamorphosed porous chromite. Based upon temperature modelling, the same authors concluded that qualitative assessment of temperature can be applied in metamorphosed spinel grains. In the present study the preserved cores record on average 1,636 ppm of ZCM, whereas porous rims concentrate 2,633 ppm. These contents are comparable with those in the case of East Rhodope (2,772 ppm; Gervilla et al., 2012; Colás et al., 2014), with temperatures ranging between 450–700°C, pointing to amphibolite facies. These metamorphic conditions were also reported for the case 1) of re-equilibrated Nea Roda chromitites (Bussolesi et al., 2022a), and b) the Askos meta-ultramafics (adjacent to the Volvi occurrence) at 0.4 GPa and 450–550°C (Michailidis, 1991). Therefore, the SMM-hosted occurrences of Gomati and Nea Roda have undergone amphibolite facies metamorphism coinciding with the RM meta-ophiolites.

5.4 Magmatic *versus* post-magmatic PGE distribution and mineralization

In ophiolites, arc-related melts produced in SSZ settings require high degrees of partial melting of a mantle source to develop chromitites enriched in PGE, especially for refractory IPGE, up to a few thousand ppb (Economou-Eliopoulos, 1996; González-Jiménez et al., 2011; Zaccarini et al., 2011). Lower degrees of partial melting account for only a small portion of melt, leading to PGE-poor chromitites yet relatively enriched in the less refractory PPGE (Economou-Eliopoulos, 1996; González-Jiménez et al., 2011 and references therein). PPGE/IPGE ratios are consistently low for the G2 and NR Cr-rich chromitites with an average of 0.24 unlike the G1 chromitite with average ratios of 0.93. Previous studies refer to ratios of 0.07 and 0.23 for Cr- and Al-rich chromitites of Gomati, respectively (Economou-Eliopoulos, 1996; Bussolesi et al., 2022b). Yet, the similar PGE patterns of the compositionally different chromitites studied may be interpreted as products of continuous melt production from a common source (Rollinson, 2005). This would have led to gradual depletion of the initially fertile mantle and its modification into a harzburgite residue that became enriched in PGE-bearing sulfides, dominated by IPGE, following the initial removal of PPGE (Büchl et al., 2002). Indeed, the studied chromitites display a gradual enrichment in IPGE and ΣPGE from the G1 towards NR and G2 occurrences. The average ΣPGE contents demonstrate a decrease from G2-245.0 to NR-154.6 and to G1-98.8 (collective data: this study; Economou-Eliopoulos, 1996; Bussolesi et al., 2022b). This trend has been previously described by Uysal et al. (2016) referring to chromitites produced by a successively fractionating melt with deeper-crystallized Cr-rich chromitites being more enriched when compared to the more shallow "intermediate" counterparts.

The higher Pd/Ir ratios (>1) of the G1 and one sample of G2 chromitites can be interpreted *via* two scenarios: 1) enrichment of PPGE due to metasomatic processes or 2) due to fractional crystallization (Garuti et al., 1997 and references therein). The first scenario, although plausible in principle, is supported by only one piece of evidence, which is the presence of a single secondary Pd-Sb PGM within the G1 chromitite. The analyzed primary PGM from the Gomati chromitites (subhedral laurite included in chromite) contain no appreciable PPGE and this agrees with findings by Bussolesi et al. (2022b). Irarsite was encountered in all chromitites. In the NR chromitites, primary laurite appears modified (Tarkian and Prichard, 1987; Zaccarini et al., 2005) with high arsenic contents and oscillatory zoning (euhedral to subhedral included in chromite) along with Pt-As-bearing secondary platarsite and sperrylite (crystallized in chlorite matrix) which do not greatly affect the low PPGE/IPGE ratios of NR chromitites. Therefore, we attribute the Pd/Ir enrichments of G1 and G2 to parental melt fractionation and not to alteration processes. Based on asthenospheric mantle-normalized PGE concentrations, low $Pt/Pt^* = Pt_N/(Rh_N \times Pd_N)^{1/2}$ ratios (<1) (Figure 10B) are consistent with increasing degrees of partial melting of the mantle source, which seems to be the main mechanism that control the PGE distribution since the elevated Pd/Ir ratios were only encountered in four out of twenty nine

samples from chromitites of SMM and RM. The generally low Pt/Pt* ratios point to a residual mantle source (Garuti et al., 1997).

5.5 LREE-Sb-As enrichments and their relationship with subduction-related serpentinization

Taking into consideration the secondary and modified primary PGM, as well as other base metals that were encountered (Ni-Sb) as also reported by Bussolesi et al. (2020, 2022b), it is evident that there is an enrichment in As + Sb during a post-magmatic event. Bussolesi et al. (2020, 2022b) assigned this metasomatism to the 53–55 Ma Ierissos pluton intrusion or porphyry copper related mineralization. However, no alteration effects related to the metallogenesis of Kassandra district have been reported for the Ierissos pluton as well as along the 12 km Gomati Fault (Siron et al., 2018 and references therein). The Kassandra metallogenesis is linked to two temporally distinct intrusions ranging between 25–27 and 19–20 Ma, situated more than 5 km NW from Gomati ultramafic bodies (Siron et al., 2018 and references therein). Therefore, the aforementioned enrichments should be attributed to a more widespread event. The best fitting scenario is the effect of pervasive serpentinization, evident in all the ultramafic lithologies. Geochemical analysis of the serpentinites with respect to the Gomati Ni-Sb-As-bearing mineralization, demonstrate enrichments in those elements, typically originating from contamination of sedimentary origins (Deschamps et al., 2011; Koutsovitis, 2017). These characteristics, combined with the elevated contents of Cs, U and Ba point to serpentinites related to a subduction zone (Deschamps et al., 2013). According to Deschamps et al. (2013 and references therein) the protolith of such serpentinites may be: 1) subduction-related oceanic peridotites or 2) OCT-related continental peridotites that were exhumed and altered during rifting. The LREE enrichments in serpentinites are considered to have derived from a process of fluid circulation within SSZ environment (Deschamps et al., 2013; Xie et al., 2021), although arguably an already metasomatized protolith could also display the same enrichments (Deschamps et al., 2013).

LREE enrichments are recorded in the diopside hosted within G1-chromitites and diopsidites. In general, primary diopside related to such rocks is expected to demonstrate LREE depletion. G1 diopsidite veins are metasomatic products based on titanite chemistry (Supplementary Figure S3; metamorphic and not magmatic affinity: Ling et al., 2015; Kiss and Zaccarini, 2020), and diopside chemistry is similar to the Omani metasomatic diopsidites (major elements: Figure 6A and HREE Figure 6C; Python et al., 2011; Arai et al., 2020). Diopside within G1 chromitite is comparable with diopside hosted within the Al-rich subduction initiation-related chromitite of Moa-Baracoa (major elements: Figure 6A and HREE Figure 6C). However, Rui et al. (2022) argue that these diopsides are not syngenetic with the chromitites. Moreover, Zhang et al. (2016) attribute LREE enrichments in clinopyroxene hosted in subduction-initiation related dunite and Cr-chromitites (demonstrating concave spoon-shaped patterns) to their post-magmatic equilibration with metasomatic fluids derive from the subducted slab. Therefore, the diopside hosted in G1 chromitites is also a metasomatic affected phase.

LREE, for both diopside types as reported in this study, are generally enriched and their convex upward patterns are often interpreted as due to interaction with alkaline melts (Matusiak-Małek et al., 2021); yet, no alkali basalts occurrences were located in the field nor K-bearing minerals have crystallized. However, similar patterns could be due to fluid metasomatism; negative Nb, P and Ti anomalies are noted in SSZ-related rocks, which are usually ascribed to reaction with hydrous fluids within the mantle (Walker and Cameron, 1983; Tatsumi and Eggins, 1995; Horodyskyj et al., 2009; Guice et al., 2018). In such cases, H_2O and CO_2-rich hydrothermal fluids can favor LREE mobilization relatively to HFSE within subduction zone settings (Walker and Cameron, 1983; Guice et al., 2018). Amphibolitization (Guice et al., 2018) and serpentine-eclogite interaction (Horodyskyj et al., 2009) within serpentinite channels, can control such remobilization. Another important aspect of the studied diopside is the positive Pb anomalies, which are a feature of serpentinites and subducted oceanic crusts (Horodyskyj et al., 2009; Deschamps et al., 2011; Cruciani et al., 2017). Subduction-related fluid metasomatism likely influenced significantly the diopsidites since their diopside grains accumulate higher concentrations of FME and LILE. The low Zr/Hf ratios of the clinopyroxene hosted within the titanite bearing diopsidite is likely attributed to the preference of Zr entering the titanite rather than clinopyroxene (Bea et al., 2006). From the above it is evident that post-magmatic subduction related fluids have altered the primary trace element composition of the studied mineral phases.

5.6 Cr-ore genesis and post-magmatic modification in the TVG complex

The TVG complex, along with other meta-ophiolitic occurrences within RM, has a rather complex geological history. The podiform chromitites display bimodal character with coexistence of Cr- and Al-rich chromitites within the same section. To our knowledge, no tectonic structure exists that could juxtapose those different sections. Hence, the proposed geotectonic model should account for the genesis of those chromitites within the same geotectonic context. Subduction initiation is considered by many researchers as a key process in the evolution of plate tectonics that can also adequately explain the genesis of Al-chromitites with mixed MORB and arc characteristics. However, the mineral products

(spinel, diopside) of this environment appear typically Ti-poor (Zhang et al., 2016; Rui et al., 2022) when compared to the mineral components of the G1 chromitite. Therefore, it is suggested that the G1 chromitites were formed from a MORB-like melt produced in extensional settings, as has also been proposed for the RM-hosted meta-chromitites of Dobromirtsi (González-Jiménez et al., 2015). The extensional phase is followed by oceanic closure, whereas the pre-existing mantle section is introduced into SSZ settings (Uysal et al., 2009), translating into higher degrees of partial melting and subsequent depletion of the mantle source. The ensuing chromitites are thus Cr-rich, represented by the G2 and NR chromitite end members. In this light, the SSZ NR chromitites could represent a product of fractionation of the previously Cr-rich G2 since they are Al-richer (Figure 4B) (Zaccarini et al., 2011; Uysal et al., 2016).

Along with the gradual maturation of the subduction zone, fluids liberated from the subduction channel brought about serpentinization and interaction with diopside resulting into LREE enrichments, accompanied by depletion in Nb-Ta, Zr, Ti and increase in Pb. The peak of metamorphism reached amphibolite facies while porous chromite was formed (450°C–700°C). During the regional extensional deformation, the chromitites experienced a greenschist facies overprint (Siron et al., 2018 and references therein) and garnet was crystallized within shear and brecciated zones at temperatures <400 C. Solutions enriched in Fe^{3+} interacted with the porous chromite creating Fe^{3+} enriched chromite and magnetite. Chlorite was re-equilibrated at temperatures <300 C. Secondary PPGE-rich PGM and As-Sb bearing minerals were observed within the chlorite matrix, representing a low-T stage (greenschist facies) whereby PPGE mobile (Tsikouras et al., 2006; Farré-de-Pablo et al., 2021) and As-Sb were incorporated during serpentinization due to input from a sedimentary source (Deschamps et al., 2011; Koutsovitis, 2017).

6 Conclusion

The meta-ultramafic sections of the TVG complex host bimodal chromitites. The Gomati occurrences host Al-rich chromitites and the most Cr-enriched chromitites of the complex, whereas the Nea Roda counterparts are compositionally intermediate to these compositions. Spinels display porous rims, with an inner rim surrounding the pristine core while in some cases mosaic textures were noted. Chromites are generally less susceptible to alteration, manifested at the first alteration stage through Fe^{2+} followed by Fe^{3+} enrichments in non-massive chromitites. The MORB-normalized trace element patterns of pristine G1 compositions are mostly flat, with negative Sc and Ni behavior. The pristine G2 and most-likely re-equilibrated NR patterns demonstrate positive trends with a positive Ti and negative Ni anomaly. These patterns are similar with those of back-arc generated chromitites of the RM. Alteration causes enrichment in ZCM. Based on the unaltered core analyses the spinel-group minerals, as well as their parental melts, the G1 present MOR and the G2-NR boninitic affinities, respectively.

The PGE chondrite-normalized patterns are typical of Tethyan podiform chromitites with Ru positive anomalies. ΣPGE contents are decreasing from the G2 to NR and finally to G1, maintaining comparable patters. The Pd/Ir ratios >1 reported in the present study are mainly attributed to fractionation rather than secondary processes. This is supported by our observations of primary and modified laurite and a few grains of secondary PPGE minerals, that seem to have a nugget effect on the ΣPGE contents, but clearly mark the effect of PPGE remobilization during low-T alteration. High Mg# diopsides hosted within G1 chromitites either as interstitial phases or as a part of cross-cutting diopsidite veins exhibit LREE-Pb enrichments and negative Nb-Ta and Ti anomalies in their normalized patterns. These signatures, coupled with enrichments in LREE and Sb-As in serpentinites (and Sb-As mineralization in chromitites) point to serpentinization within a subduction zone and reaction of diopsides with SSZ-derived fluids. Temperature estimations based upon garnet, chlorite and spinel chemistry revealed that the ultramafic TVG sections have reached amphibolite facies later overprinted by greenschist assemblages. The chromitites were most likely formed in a back-arc affected by SSZ activity and subsequent metamorphism within a subduction zone.

Data availability statement

The original contributions presented in the study are included in the article/Supplementary Material, further inquiries can be directed to the corresponding author.

Author contributions

All authors listed have made a substantial, direct, and intellectual contribution to the work and approved it for publication. AS wrote the manuscript, contributed to the fieldwork, prepared the samples, acquired the majority of datasets, interpreted the data and completed illustrations. BT, PT and KH took part in the fieldwork preparation and sampling. PT aided in the preparation and selection of the representative samples. BT, PK, FZ, CH, HT and KH aid in the interpretation of the data and offered a critical review on the scientific content and English language of the manuscript. FZ and CH contributed to data acquisition and calibration of the analytical equipment. PK aided in the illustration.

Funding

This research work was supported by the Hellenic Foundation for Research and Innovation (HFRI) under the

HFRI PhD Fellowship grant (Fellowship Number: 1616), obtained by AS to conduct his PhD Thesis. The publication fees of this manuscript have been financed by the Research Council of the University of Patras.

Acknowledgments

The University Centrum for Applied Geosciences (UCAG) is thanked for offering access to the Eugen F. Stumpfl electron microprobe Laboratory. Erasmus+ for traineeships is also thanked for providing the opportunity to AS to perform analyses at the Eugen F. Stumpfl Electron Microprobe Laboratory and LA-ICP-MS facility at the NAWI Graz Central Lab for Water, Minerals and Rocks. SGS Mineral Services (Canada) and Dr. Tassos Grammatikopoulos are thanked for performing the chromitite concentrates. Luca Bindi is thanked for his contribution to the identification of the Ni grain enriched in phosphorous. We are thankful to the Editor and Reviewers for helping ameliorate the final version of the manuscript.

Conflict of interest

The authors declare that the research was conducted in the absence of any commercial or financial relationships that could be construed as a potential conflict of interest.

Publisher's note

Supplementary material

The Supplementary Material for this article can be found online at: https://www.frontiersin.org/articles/10.3389/feart.2022.1031239/full#supplementary-material

References

Akbulut, M., González-Jiménez, J. M., Belousova, E., Ginés, V. C., de Pablo, J. F., Solà, N. P., et al. (2022). A record of metasomatism and crustal contamination of the Mediterranean lithosphere in chromitites of the Orhaneli Ophiolite Complex (NW Türkiye). *J. Asian Earth Sci.* 236, 105311. doi:10.1016/j.jseaes.2022.105311

Akbulut, M., González-Jiménez, J. M., Griffin, W. L., Belousova, E., O'Reilly, S. Y., McGowan, N., et al. (2016). Tracing ancient events in the lithospheric mantle: A case study from ophiolitic chromitites of SW Turkey. *J. Asian Earth Sci.* 119, 1–19. doi:10.1016/j.jseaes.2016.01.008

Arai, S., Kadoshima, K., and Morishita, T. (2006). Widespread arc-related melting in the mantle section of the northern Oman ophiolite as inferred from detrital chromian spinels. *J. Geol. Soc. Lond.* 163, 869–879. doi:10.1144/0016-76492005-057

Arai, S., Miura, M., Tamura, A., Akizawa, N., and Ishikawa, A. (2020). Hydrothermal chromitites from the Oman ophiolite: The role of water in chromitite Genesis. *Minerals* 10, 217. doi:10.3390/min10030217

Barnes, S. J., and Roeder, P. L. (2001). The range of spinel compositions in terrestrial mafic and ultramafic rocks. *J. Petrol.* 42, 2279–2302. doi:10.1093/petrology/42.12.2279

Bea, F., Montero, P., and Ortega, M. (2006). A LA-ICP-MS evaluation of Zr reservoirs in common crustal rocks: Implications for Zr and Hf geochemistry, and zircon-forming processes. *Can. Mineralogist* 44, 693–714. doi:10.2113/gscanmin.44.3.693

Bonev, N., and Dilek, Y. (2010a). Geochemistry and tectonic significance of proto-ophiolitic metamafic units from the Serbo-Macedonian and Western Rhodope massifs (Bulgaria-Greece). *Int. Geol. Rev.* 52, 298–335. doi:10.1080/00206810902757214

Bonev, N., and Dilek, Y. (2010b). Geochemistry and tectonic significance of proto-ophiolitic metamafic units from the Serbo-Macedonian and Western Rhodope massifs (Bulgaria-Greece). doi:10.1080/00206810902757214

Bonev, N., Moritz, R., Borisova, M., and Filipov, P. (2018). Therma–volvi–gomati complex of the serbo-Macedonian massif, northern Greece: A middle triassic continental margin ophiolite of neotethyan origin. *J. Geol. Soc. Lond.* 176, 931–944. doi:10.1144/jgs2017-130

Bosi, F., Biagioni, C., and Pasero, M. (2019). Nomenclature and classification of the spinel supergroup. *Eur. J. Mineral.* 31, 183–192. doi:10.1127/ejm/2019/0031-2788

Büchl, A., Brügmann, G., Batanova, V. G., Münker, C., and Hofmann, A. W. (2002). Melt percolation monitored by Os isotopes and hse abundances: A case study from the mantle section of the troodos ophiolite. *Earth Planet. Sci. Lett.* 204, 385–402. doi:10.1016/S0012-821X(02)00977-9

Bussolesi, M., Grieco, G., Cavallo, A., and Zaccarini, F. (2022a). Different tectonic evolution of fast cooling ophiolite mantles recorded by olivine-spinel geothermometry: Case studies from iballe (Albania) and Nea Roda (Greece). *Minerals* 12, 64. doi:10.3390/min12010064

Bussolesi, M., Grieco, G., Zaccarini, F., Cavallo, A., Tzamos, E., and Storni, N. (2022b). Chromite compositional variability and associated PGE enrichments in chromitites from the Gomati and Nea Roda ophiolite, Chalkidiki, Northern Greece. *Min. Depos.* 57, 1323–1342. doi:10.1007/s00126-022-01109-z

Bussolesi, M., Zaccarini, F., Grieco, G., and Tzamos, E. (2020). Rare and new compounds in the Ni-Cu-Sb-As system: First occurrence in the Gomati ophiolite, Greece. *Period. Miner.* 89, 63–76. doi:10.2451/2020PM893

Cathelineau, M. (1988). Cation site occupancy in chlorites and illites as a function of temperature. *Clay Min.* 23, 471–485. doi:10.1180/claymin.1988.023.4.13

Cathelineau, M., and Nieva, D. (1985). A chlorite solid solution geothermometer the Los Azufres (Mexico) geothermal system. *Contr. Mineral. Petrol.* 91, 235–244. doi:10.1007/BF00413350

Chen, C., Su, B.-X. B.-X., Xiao, Y., Pang, K.-N. K.-N., Robinson, P. T. P. T., Uysal, I., et al. (2019). Intermediate chromitite in Kızıldağ ophiolite (SE Turkey) formed during subduction initiation in Neo-Tethys. *Ore Geol. Rev.* 104, 88–100. doi:10.1016/j.oregeorev.2018.10.004

Christodoulou, C., and Hirst, D. M. M. (1985). The chemistry of chromite from two mafic-Ultramafic complexes in northern Greece. *Chem. Geol.* 49, 415–428. doi:10.1016/0009-2541(85)90003-8

Christodoulou, C. (1980). *The Geochemistry of podiform chromite deposits from two ophiolite complexes. Northern Greece, Chalkidiki Peninsula*.

Colás, V., González-Jiménez, J. M., Camprubí, A., Proenza, J. A., Griffin, W. L., Fanlo, I., et al. (2019). A reappraisal of the metamorphic history of the Tehuitzingo chromitite, Puebla state, Mexico. *Int. Geol. Rev.* 61, 1706–1727. doi:10.1080/00206814.2018.1542633

Colás, V., González-Jiménez, J. M., Griffin, W. L., Fanlo, I., Gervilla, F., O'Reilly, S. Y., et al. (2014). Fingerprints of metamorphism in chromite: New insights from minor and trace elements. *Chem. Geol.* 389, 137–152. doi:10.1016/j.chemgeo.2014.10.001

Cruciani, G., Franceschelli, M., and Puxeddu, M. (2017). U-Pb-enrichment, Sr-depletion produced by water-rock interaction processes within the eclogitic oceanic crust of ordovician age in NE sardinia. *Procedia Earth Planet. Sci.* 17, 508–511. doi:10.1016/j.proeps.2016.12.128

de Melo Portella, Y., Zaccarini, F., Luvizotto, G. L., Garuti, G., Bakker, R. J., Angeli, N., et al. (2016). The cedrolina chromitite, goiás state, Brazil: A metamorphic puzzle. *Minerals* 6, 91. doi:10.3390/min6030091

Deschamps, F., Godard, M., Guillot, S., and Hattori, K. (2013). Geochemistry of subduction zone serpentinites: A review. *Lithos* 178, 96–127. doi:10.1016/j.lithos.2013.05.019

Deschamps, F., Guillot, S., Godard, M., Andreani, M., and Hattori, K. (2011). Serpentinites act as sponges for fluid-mobile elements in abyssal and subduction zone environments. *Terra Nov.* 23, 171–178. doi:10.1111/j.1365-3121.2011.00995.x

Dick, H. J. B., and Bullen, T. (1984). Chromian spinel as a petrogenetic indicator in abyssal and alpine-type peridotites and spatially associated lavas. *Contr. Mineral. Petrol.* 86, 54–76. doi:10.1007/BF00373711

Dixon, J. E., and Dimitriadis, S. (1984). *Metamorphosed ophiolitic rocks from the serbo-Macedonian massif, near lake Volvi, north-east Greece*. doi:10.1144/GSL.SP.1984.017.01.47

Economou-Eliopoulos, M. (1996). Platinum-group element distribution in chromite ores from ophiolite complexes: Implications for their exploration. *Ore Geol. Rev.* 11, 363–381. doi:10.1016/S0169-1368(96)00008-X

Falloon, T. J., Danyushevsky, L. V., Crawford, A. J., Meffre, S., Woodhead, J. D., and Bloomer, S. H. (2008). Boninites and adakites from the northern termination of the Tonga Trench: Implications for adakite petrogenesis. *J. Petrology* 49, 697–715. doi:10.1093/petrology/egm080

Farré-de-Pablo, J., Proenza, J. A., González-Jiménez, J. M., Aiglsperger, T., Torró, L., Domènech, C., et al. (2021). Low-temperature hydrothermal Pt mineralization in uvarovite-bearing ophiolitic chromitites from the Dominican Republic. *Min. Depos.* 57, 955–976. doi:10.1007/s00126-021-01079-8

Garuti, G., Fershtater, G., Bea, F., Montero, P., Pushkarev, E. V. V., and Zaccarini, F. (1997). Platinum-group elements as petrological indicators in mafic-ultramafic complexes of the central and southern Urals: Preliminary results. *Tectonophysics* 276, 181–194. doi:10.1016/S0040-1951(97)00050-4

Gervilla, F., Padrón-Navarta, J. A., Kerestedjian, T., Sergeeva, I., González-Jiménez, J. M., and Fanlo, I. (2012). formation of ferrian chromite in podiform chromitites from the golyamo kamenyane serpentinite, eastern rhodopes, se Bulgaria: A two-stage process. *Contrib. Mineral. Petrol.* 164, 643–657. doi:10.1007/s00410-012-0763-3

González-Jiménez, J. M., Locmelis, M., Belousova, E., Griffin, W. L., Gervilla, F., Kerestedjian, T. N., et al. (2015). Genesis and tectonic implications of podiform chromitites in the metamorphosed ultramafic massif of Dobromirtsi (Bulgaria). *Gondwana Res.* 27, 555–574. doi:10.1016/j.gr.2013.09.020

González-Jiménez, J. M., Proenza, J. A., Gervilla, F., Melgarejo, J. C., Blanco-Moreno, J. A., Ruiz-Sánchez, R., et al. (2011). High-Cr and high-Al chromitites from the Sagua de Tánamo district, Mayarí-Cristal ophiolitic massif (eastern Cuba): Constraints on their origin from mineralogy and geochemistry of chromian spinel and platinum-group elements. *Lithos* 125, 101–121. doi:10.1016/j.lithos.2011.01.016

Grieco, G., Bussolesi, M., Eslami, A., Gentile, A., Cavallo, A., Lian, D., et al. (2020). Differential platinum group elements (PGE) re-mobilization at low fS_2 in Abdasht and Soghan mafic-ultramafic complexes (Southern Iran). *Lithos* 366-367, 105523–106367. doi:10.1016/j.lithos.2020.105523

Guice, G. L., McDonald, I., Hughes, H. S. R., Schlatter, D. M., Goodenough, K. M., Macdonald, J. M., et al. (2018). Assessing the validity of negative high field strength-element anomalies as a proxy for Archaean subduction: Evidence from the Ben Strome Complex, NW Scotland. *Geosci. (Basel).* 8, 338. doi:10.3390/geosciences8090338

Hey, M. H. (1954). A new review of the chlorites. *Mineral. Mag. J. Mineral. Soc.* 30, 277–292. doi:10.1180/minmag.1954.030.224.01

Himmerkus, F., Reischmann, T., and Kostopoulos, D. (2009). Serbo-Macedonian revisited: A silurian basement terrane from northern gondwana in the internal hellenides, Greece. *Tectonophysics* 473, 20–35. doi:10.1016/j.tecto.2008.10.016

Himmerkus, F., Zachariadis, P., Reischmann, T., and Kostopoulos, D. (2012). The basement of the Mount Athos peninsula, northern Greece: Insights from geochemistry and zircon ages. *Int. J. Earth Sci.* 101, 1467–1485. doi:10.1007/s00531-011-0644-4

Horodyskyj, U., Lee, C.-T. A., and Luffi, P. (2009). Geochemical evidence for exhumation of eclogite via serpentinite channels in ocean-continent subduction zones. *Geosph. (Boulder).* 5, 426–438. doi:10.1130/GES00502.1

Huang, Y., Wang, L., Robinson, P. T., Ning, W., Zhong, Y., Wang, J., et al. (2021). Podiform chromitite Genesis in an Archean juvenile forearc setting: The 2.55 Ga Zunhua chromitites, North China Craton. *Lithos* 394-395, 106194–106395. doi:10.1016/j.lithos.2021.106194

Jochum, K. P., Nohl, U., Rothbarth, N., Schwager, B., Stoll, B., and Weis, U. (2012). Geostandards and geoanalytical research bibliographic review 2011. *Geostand. Geoanal. Res.* 36, 415–419. doi:10.1111/j.1751-908X.2012.00221.x

Kamenetsky, V. S., Crawford, A. J., and Meffre, S. (2001). Factors controlling chemistry of magmatic spinel: An empirical study of associated olivine, Cr-spinel and melt inclusions from primitive rocks. *J. Petrol.* 42, 655–671. doi:10.1093/petrology/42.4.655

Kapsiotis, A., Ewing Rassios, A., Grieco, G., and Antonelou, A. (2017). Genesis of Cr-bearing hydrogrossular-rich veins in a chromitite boulder from ayios stefanos, west othris, Greece: A paradigm of micro-rodingites formation at the late stages of oceanic slab emplacement. *Ore Geol. Rev.* 90, 287–306. doi:10.1016/j.oregeorev.2017.06.006

Kapsiotis, A., Grammatikopoulos, T. A., Tsikouras, B., Hatzipanagiotou, K., Zaccarini, F., and Garuti, G. (2009). Chromian spinel composition and platinum-group element mineralogy of chromitites from the Milia area, Pindos ophiolite complex, Greece. *Can. Mineralogist* 47, 1037–1056. doi:10.3749/canmin.47.5.1037

Kiss, G. B., and Zaccarini, F. (2020). Compositional variations of titanite: A possible new tool for Cyprus-type volcanogenic massive sulfide deposit prospecting. *Geosci. (Basel).* 10, 290–311. doi:10.3390/geosciences10080290

Koutsovitis, P. (2017). High-pressure subduction-related serpentinites and metarodingites from East Thessaly (Greece): Implications for their metamorphic, geochemical and geodynamic evolution in the Hellenic–Dinaric ophiolite context. *Lithos* 276, 122–145. doi:10.1016/j.lithos.2016.11.008

Koutsovitis, P., and Magganas, A. (2016). Boninitic and tholeiitic basaltic lavas and dikes from dispersed jurassic east othris ophiolitic units, Greece: Petrogenesis and geodynamic implications. *Int. Geol. Rev.* 58, 1983–2006. doi:10.1080/00206814.2016.1198278

Kranidiotis, P., and MacLean, W. H. (1987). Systematics of chlorite alteration at the Phelps Dodge massive sulfide deposit, Matagami, Quebec. *Econ. Geol.* 82, 1898–1911. doi:10.2113/gsecongeo.82.7.1898

Kydonakis, K., Moulas, E., Chatzitheodoridis, E., Brun, J.-P., Kostopoulos, D., le Roex, A. P., et al. (2015). First-report on mesozoic eclogite-facies metamorphism preceding barrovian overprint from the Western Rhodope (Chalkidiki, northern Greece)le Roex, A., and Class, C. (2016). Metasomatic enrichment of proterozoic mantle south of the kaapvaal craton, south Africa: Origin of sinusoidal REE patterns in clinopyroxene and garnetLocal and regional heterogeneity in MORB from the mid-atlantic ridge between 54.5°S and 51°S: Evidence for geochemical enrichment. *LithosContrib. Mineral. Petrol.Geochim. Cosmochim. Acta* 220–223, 1471541–16324555. 17151. doi:10.1016/j.lithos.2015.02.00710.1007/s00410-015-1222-810.1016/0016-7037(87)90068-8

Lenaz, D., Adetunji, J., and Rollinson, H. (2014). Determination of Fe3+/ΣFe ratios in chrome spinels using a combined mössbauer and single-crystal X-ray approach: Application to chromitites from the mantle section of the Oman ophiolite. *Contrib. Mineral. Petrol.* 167, 958. doi:10.1007/s00410-013-0958-2

Lenaz, D., Skogby, H., Rigonat, N., and Berger, J. (2018). Following the amphibolite to greenschist metamorphic path through the structural parameters of spinels from amsaga (Mauritania). *Minerals* 8, 27. doi:10.3390/min8010027

Ling, X.-X., Schmädicke, E., Li, Q.-L., Gose, J., Wu, R.-H., Wang, S.-Q., et al. (2015). Age determination of nephrite by *in-situ* sims U-Pb dating syngenetic titanite: A case study of the nephrite deposit from luanchuan, henan, China. *Lithos* 220–223, 289–299. doi:10.1016/j.lithos.2015.02.019

Matusiak-Małek, M., Puziewicz, J., Ntaflos, T., Woodland, A., Uenver-Thiele, L., Büchner, J., et al. (2021). Variable origin of clinopyroxene megacrysts carried by Cenozoic volcanic rocks from the eastern limb of Central European Volcanic Province (SE Germany and SW Poland). *Lithos* 382–383, 105936. doi:10.1016/j.lithos.2020.105936

Maurel, C. (1984). *Etude experimentale de l'equilibre spinelle chromifere liquide silicate basique*.

Maurel, C., and Maurel, P. (1982). Etude experimentale de la distribution de l'aluminium entre bain silicate basique et spinelle chromifere. Implications petrogenetiques: Teneur en chrome des spinelles. *bulmi.* 105, 197–202. doi:10.3406/bulmi.1982.7605

Melcher, F., Grum, W., Simon, G., Thalhammer, T. V., and Stumpfl, E. F. (1997). Petrogenesis of the ophiolitic giant chromite deposits of kempirsai, Kazakhstan: A study of solid and fluid inclusions in chromite. *J. Petrology* 38, 1419–1458. doi:10.1093/petroj/38.10.1419

Michailidis, K. M. (1991). Fe–Cr spinel and ilmenitemassivemineralization inmetamorphic ultramafics fromthe Askos area, northern Greece. *Bull. Geol. Soc. Greece* XXV (2), 203–224.

Michailidis, K. M., and Soldatos, T. C. (1995). Ultramafic rocks and associated chromite mineralisation from Nea Roda (eastern Chalkidiki Peninsula, northern Greece). *Ofioliti* 20, 81–96.

Morimoto, N. (1988). Nomenclature of pyroxenes. *Mineral. Petrol.* 39, 55–76. doi:10.1007/BF01226262

Naldrett, A. J., and Duke, J. M. (1980). Platinum metals magmatic sulfide ores. *Science* 208, 1417–1424. doi:10.1126/science.208.4451.1417

Pagé, P., and Barnes, S.-J. (2009). Using trace elements in chromites to constrain the origin of podiform chromitites in the Thetford Mines Ophiolite, Québec, Canada. *Econ. Geol.* 104, 997–1018. doi:10.2113/gsecongeo.104.7.997

Python, M., Yoshikawa, M., Shibata, T., and Arai, S. (2011). "Diopsidites and rodingites: Serpentinisation and Ca-metasomatism in the Oman ophiolite mantle," in *Dyke swarms:keys for geodynamic interpretation* (Berlin, Heidelberg: Springer Berlin Heidelberg). doi:10.1007/978-3-642-12496-9_23

Rollinson, H., and Adetunji, J. (2013). Mantle podiform chromitites do not form beneath mid-ocean ridges: A case study from the moho transition zone of the Oman ophiolite. *Lithos* 177, 314–327. doi:10.1016/j.lithos.2013.07.004

Rollinson, H. (2005). Chromite in the mantle section of the Oman ophiolite: A new genetic model. *Isl. Arc* 14, 542–550. doi:10.1111/j.1440-1738.2005.00482.x

Rollinson, H. (2008). The geochemistry of mantle chromitites from the northern part of the Oman ophiolite: Inferred parental melt compositions. *Contrib. Mineral. Petrol.* 156, 273–288. doi:10.1007/s00410-008-0284-2

Rui, H.-C., Yang, J.-S., Llanes Castro, A. I., Zheng, J.-P., Lian, D.-Y., Wu, W.-W., et al. (2022). Ti-poor high-Al chromitites of the Moa-Baracoa ophiolitic massif (eastern Cuba) formed in a nascent forearc mantle. *Ore Geol. Rev.* 144, 104847. doi:10.1016/j.oregeorev.2022.104847

Sideridis, A., Koutsovitis, P., Tsikouras, B., Karkalis, C., Hauzenberger, C., Zaccarini, F., et al. (2022). Pervasive listwaenitization: The role of subducted sediments within mantle wedge, W. Chalkidiki ophiolites, N. Greece. *Minerals* 12, 1000. doi:10.3390/min12081000

Sideridis, A., Zaccarini, F., Grammatikopoulos, T., Tsitsanis, P., Tsikouras, B., Pushkarev, E., et al. (2018). First occurrences of ni-phosphides in chromitites from the ophiolite complexes of alapaevsk, Russia and gerakini-ormylia, Greece. *Ofioliti* 43, 75–84. doi:10.4454/ofioliti.v43i1.456

Sideridis, A., Zaccarini, F., Koutsovitis, P., Grammatikopoulos, T., Tsikouras, B., Garuti, G., et al. (2021). Chromitites from the Vavdos ophiolite (Chalkidiki, Greece): Petrogenesis and geotectonic settings; constrains from spinel, olivine composition, PGE mineralogy and geochemistry. *Ore Geol. Rev.* 137, 104289. doi:10.1016/j.oregeorev.2021.104289

Siron, C. R., Rhys, D., Thompson, J. F. H., Baker, T., Veligrakis, T., Camacho, A., et al. (2018). Structural controls on porphyry Au-Cu and Au-rich polymetallic Carbonate-hosted replacement deposits of the Kassandra mining District, Northern Greece. *Econ. Geol.* 113, 309–345. doi:10.5382/econgeo.2018.4552

Su, B., Liu, X., Chen, C., Robinson, P. T., Xiao, Y., Zhou, M., et al. (2021). A new model for chromitite formation in ophiolites: Fluid immiscibility. *Sci. China Earth Sci.* 64, 220–230. doi:10.1007/s11430-020-9690-4

Sun, S.-S., and McDonough, W. F. (1989). Chemical and isotopic systematics of oceanic basalts: Implications for mantle composition and processes. doi:10.1144/GSL.SP.1989.042.01.19

Tarkian, M., Naidenova, E., and Zhelyaskova-Panayotova, M. (1991). Platinum-group minerals in chromitites from the Eastern Rhodope ultramafic complex, Bulgaria. *Mineral. Petrol.* 44, 73–87. doi:10.1007/BF01167101

Tarkian, M., and Prichard, H. M. (1987). Irarsite-hollingworthite solid-solution series and other associated Ru-Os-Ir-and Rh-bearing PGM's from the Shetland ophiolite complex. *Min. Depos.* 22, 178–184. doi:10.1007/BF00206607

Tatsumi, Y., and Eggins, S. (1995). *Subduction zone magmatism*.

Tsikouras, B., and Hatzipanagiotou, K. (1998). Two alternative solutions for the development of a marginal basin in NE Greece. *Ofioliti* 23, 83–92.

Tsikouras, B., Karipi, S., Grammatikopoulos, T. A., and Hatzipanagiotou, K. (2006). Listwaenite evolution in the ophiolite mélange of Iti Mountain (continental Central Greece). *Eur. J. Mineral.* 18, 243–255. doi:10.1127/0935-1221/2006/0018-0243

Tsoupas, G., and Economou-Eliopoulos, M. (2008). High PGE contents and extremely abundant PGE-minerals hosted in chromitites from the Veria ophiolite complex, northern Greece. *Ore Geol. Rev.* 33, 3–19. doi:10.1016/j.oregeorev.2006.10.008

Uysal, I., Akmaz, R. M., Saka, S., and Kapsiotis, A. (2016). Coexistence of compositionally heterogeneous chromitites in the antalya-isparta ophiolitic suite, SW Turkey: A record of sequential magmatic processes in the sub-arc lithospheric mantle. *Lithos* 248–251, 160–174. doi:10.1016/j.lithos.2016.01.021

Uysal, I., Tarkian, M., Sadiklar, M. B., Zaccarini, F., Meisel, T., Garuti, G., et al. (2009). Petrology of Al- and Cr-rich ophiolitic chromitites from the muğla, SW Turkey: Implications from composition of chromite, solid inclusions of platinum-group mineral, silicate, and base-metal mineral, and Os-isotope geochemistry. *Contrib. Mineral. Petrol.* 158, 659–674. doi:10.1007/s00410-009-0402-9

Walker, D. A., and Cameron, W. E. (1983). Boninite primary magmas: Evidence from the cape vogel peninsula, PNG. *Contr. Mineral. Petrol.* 83, 150–158. doi:10.1007/BF00373088

Xie, Z., Hattori, K., Dong, Y., and Wang, J. (2021). *In situ* characterization of forearc serpentinized peridotite from the Sulu ultrahigh-pressure terrane: Behavior of fluid-mobile elements in continental subduction zone. *Geosci. Front.* 12, 101139. doi:10.1016/j.gsf.2021.101139

Xiong, F., Yang, J., Dilek, Y., Wang, C. L., Hao, X., Xu, X., et al. (2018). Petrology and geochemistry of the high-Cr podiform chromitites of the köycegiz ophiolite, southwest Turkey: Implications for the multi-stage evolution of the oceanic upper mantle. *Mineral. Petrol.* 112, 685–704. doi:10.1007/s00710-018-0560-4

Xiong, F., Zoheir, B., Wirth, R., Milushi, I., Qiu, T., and Yang, J. (2021). Mineralogical and isotopic peculiarities of high-Cr chromitites: Implications for a mantle convection Genesis of the Bulqiza ophiolite. *Lithos* 398-399, 106305–106399. doi:10.1016/j.lithos.2021.106305

Xiong, Q., Henry, H., Griffin, W. L., Zheng, J.-P. J. P., Satsukawa, T., Pearson, N. J. N. J., et al. (2017). High- and low-Cr chromitite and dunite in a Tibetan ophiolite: Evolution from mature subduction system to incipient forearc in the neo-tethyan ocean. *Contrib. Mineral. Petrol.* 172, 45–22. doi:10.1007/s00410-017-1364-y

Yao, S. (1999). *Chemical composition of chromites from ultramafic rocks: Application to mineral exploration and petrogenesis*.

Zaccarini, F., Bindi, L., Ifandi, E., Grammatikopoulos, T., Stanley, C., Garuti, G., et al. (2019). Tsikourasite, Mo3Ni2P1+x (x < 0.25), a new phosphide from the chromitite of the othrys ophiolite, Greece. *Minerals* 9, 248. doi:10.3390/min9040248

Zaccarini, F., Garuti, G., Proenza, J. A., Campos, L., Thalhammer, O. A. R., Aiglsperger, T., et al. (2011). Chromite and platinum group elements mineralization in the santa elena ultramafic nappe (Costa Rica): Geodynamic implications. *Geol. Acta* 9, 407–423. doi:10.1344/105.000001696

Zaccarini, F., Proenza, J. A., Ortega-Gutiérrez, F., and Garuti, G. (2005). Platinum group minerals in ophiolitic chromitites from Tehuitzingo (Acatlán complex, southern Mexico): Implications for post-magmatic modification. *Mineral. Petrol.* 84, 147–168. doi:10.1007/s00710-005-0075-7

Zang, W., and Fyfe, W. S. (1995). Chloritization of the hydrothermally altered bedrock at the Igarap Bahia gold deposit, Carajs, Brazil. *Min. Depos.* 30, 30–38. doi:10.1007/BF00208874

Zhang, P.-F., Uysal, I., Zhou, M.-F., Su, B.-X., and Avcı, E. (2016). Subduction initiation for the formation of high-Cr chromitites in the Kop ophiolite, NE Turkey. *Lithos* 260, 345–355. doi:10.1016/j.lithos.2016.05.025

Zhou, M. F. F., Robinson, P. T. T., and Bai, W. J. J. (1994). Formation of podiform chromitites by melt/rock interaction in the upper mantle. *Min. Depos.* 29, 98–101. doi:10.1007/BF03326400

Zhou, M. F., Robinson, P. T., Su, B. X., Gao, J. F., Li, J. W., Yang, J. S., et al. (2014). Compositions of chromite, associated minerals, and parental magmas of podiform chromite deposits: The role of slab contamination of asthenospheric melts in suprasubduction zone environments. *Gondwana Res.* 26, 262–283. doi:10.1016/j.gr.2013.12.011